Reconstructive adsorption of Na on Al(111) studied by scanning tunneling microscopy

H. Brune,* J. Wintterlin, R. J. Behm,† and G. Ertl

Fritz-Haber-Institut der Max-Planck-Gesellschaft, Faradayweg 4-6, D-14195 Berlin, Germany

(Received 28 July 1994)

We present a scanning-tunneling-microscopy (STM) study of the adsorption behavior of Na on Al(111) at room temperature. For this system, a reconstruction of the close-packed metal surface is realized for both ordered structures, the $(\sqrt{3} \times \sqrt{3})R\,30°$ structure with $\Theta = 0.33$ and the (2×2) phase with $\Theta = 0.50$. For the first one, this leads to properties that are quite uncommon for alkali metals on close-packed metal surfaces and that are detectable by STM: island formation already for low coverages, structure-selective nucleation at Al step edges, and a low adsorbate mobility corresponding to a diffusion coefficient of $D = 10^{-14}$ cm^2 s^{-1} at $T = 300$ K. The mobile species is identified as a Na atom residing in a substrate vacancy (substitutional Na). For the diffusion mechanism, a concerted motion of Na and the underlying vacancy is proposed. The adsorption site of Na was found to be in registry with the Al lattice. These findings confirm the reconstruction model recently proposed for Na in the $(\sqrt{3} \times \sqrt{3})R\,30°$ structure, in which Na atoms are adsorbed above vacancies in the Al(111) surface, i.e., on substitutional sites. Upon further uptake of Na, the domain walls of the $(\sqrt{3} \times \sqrt{3})R\,30°$ structure change from light to heavy walls. The latter are the nuclei for the (2×2) phase. This phase has two Na atoms per unit cell. Nevertheless, it is characterized by a single protrusion per unit cell in the STM images, and a sixfold rotational symmetry. On large terraces the mass transport involved in the phase transition $(\sqrt{3} \times \sqrt{3})R\,30° \rightarrow (2 \times 2)$ is analyzed, from which a number of three Al surface atoms per unit cell of the (2×2) phase was derived. This leads to a structure model for the (2×2) phase where one Na atom is adsorbed on a substitutional site as in the lower coverage $(\sqrt{3} \times \sqrt{3})R\,30°$ structure and the second Na atom resides on the hollow sites of the mixed Na-Al layer. This bilayer model explains the thermal-desorption characteristics and exhibits only a single Na-Al bond length of 3.3 Å, in agreement with recent surface-extended x-ray-absorption fine-structure results. A similar model with one additional Al atom recently proposed is discussed in context with the present STM data.

I. INTRODUCTION

The physical and chemical properties of metal surfaces are significantly changed by the adsorption of alkali metals. It has been observed already in the last century that adsorbed alkali metals enhance the catalytic activity of platinum surfaces.[1] For tungsten electrodes alkali-metal adsorption has been found to drastically enhance the electron emission.[2] Since these early observations, alkali-metal adsorption has been a topic of current interest, which is partly due to the technological importance of alkali-metal adsorbates, for instance, in heterogeneous catalysis and for the production of efficient emitters. From a scientific point of view, alkali-metal atoms are, due to their simple electronic structure, ideal candidates for model chemisorption studies. The standard description of alkali-metal adsorption goes back to Taylor, Langmuir, and Gurney.[2,3] In the Langmuir-Gurney model, the alkali-metal atom transfers—at low coverages—most of its valence-electron density to the metal substrate. As a consequence, a dipole is formed by the alkali ion and its image charge in the surface. It points from the bulk to the vacuum, which explains the work function decrease and hence the increase in electron emission.[4] This classical picture of alkali-metal adsorption has been questioned in the recent past. Theoretical studies concluded that the alkali-metal atom is, in fact, covalently bound and that the dipole moment is rather

due to an internal polarization than to an ionic bond.[5,6] These findings were supported by x-ray photoelectron spectroscopy (XPS) experiments.[7,8] Although the appropriate description of the alkali-metal chemisorption bond is a matter of an ongoing debate, a recent investigation came to the conclusion that the apparent discrepancy is more semantic in nature and that the original concept still has its validity.[9,10]

Apart from the character of the bond to the substrate, the adsorption geometry of the alkali-metal atoms turned out to be a more complex issue than originally believed. So far it has been tacitly assumed that alkali-metal atoms on close-packed metal surfaces would always occupy the threefold coordinated hollows. Whereas this is actually the case for many systems, a number of cases were reported recently where the alkali-metal atoms occupy on-top sites.[11-13] Another case where experimental results strongly contrast the expectation is represented by the adsorption of sodium on Al(111), in particular, in view of the jellium character of this surface. The sequence of ordered structures typical for other close-packed surfaces, a (2×2) followed by a $(\sqrt{3} \times \sqrt{3})R\,30°$ structure, is reversed here, and the characteristic "ring phase" at low coverages is absent. Most surprisingly, recent SEXAFS (surface extended x-ray-absorption fine-structure) experiments showed that a reconstruction is involved in the $(\sqrt{3} \times \sqrt{3})R\,30°$ phase. Every third Al atom is removed from the surface layer and replaced by Na.[14] Although

reconstructions are well known for alkali-metal adsorption on the more open (110) surfaces of fcc metals as Cu, Ni, Ag, and Pd,[15] they have not been expected for close-packed surfaces. This was even more surprising for the case of aluminum, which is completely immiscible with sodium in the bulk.[16] The reconstruction can, therefore, not be considered as a first step towards an alloy, as it has been done, e.g., for Na/Au(111).[17] However, *ab initio* density-functional calculations showed that such a type of reconstruction is indeed energetically favorable for that system.[14,18] This peculiar adsorption geometry in the $(\sqrt{3} \times \sqrt{3})R\,30°$ room-temperature structure of Na on Al(111) has been confirmed by a recent LEED-IV analysis[19] as well as by a standing x-ray wave-field absorption study[13,20] and is in agreement with conclusions from x-ray experiments.[21,22]

In this paper, we present scanning-tunneling-microscopy (STM) results which give direct evidence for substitutional adsorption for Na in the $(\sqrt{3} \times \sqrt{3})R\,30°$ structure formed on Al(111) at $T = 300$ K. We find that this unique adsorption geometry has a number of implications which have been postulated from theory,[18] but for which only little or no experimental evidence existed. They are quite uncommon for alkali-metal adsorption: First, island formation already at very low coverages is clear evidence of an attractive interaction between the alkali-metal atoms (on their reconstructed adsorption sites). Second, steps play an important role in the nucleation of this phase. Furthermore, the STM images give evidence for a unique diffusion mechanism consisting of the combined migration of a substrate vacancy and the adsorbed Na atom.

The structure of the (2×2) phase, which is formed upon increasing the Na coverage beyond that of the $(\sqrt{3} \times \sqrt{3})R\,30°$ structure, has been a matter of debate in recent literature. From its coverage of 0.5 [coverages are given as a ratio of the density of adatoms over that of the Al(111) plane] it must be different from the simple (2×2) phases known from other close-packed surfaces with $\Theta = 0.25$ and the alkali-metal atoms sitting in hollow sites. Originally, a structure consisting of three domains of a (2×1) phase was proposed.[23] From the STM observations for the (2×2) phase this model can be ruled out. The first (2×2) double-layer model was introduced by Hohlfeld and Horn, which consists of a distorted double layer of bcc Na(111) lattice planes.[24] However, from the STM data presented below, we can directly conclude that a reconstruction is involved in the (2×2) structure, which is likely because it develops from the $\sqrt{3}$ phase, which itself involves reconstruction. This is in accordance with XPS data, which show that intermixing takes place.[21,22] A standing x-ray-absorption study came to a reconstruction model of a bilayer of Al_2Na consistent with the core-level spectra.[13,20] Here we derive a different model from the mass balance of the Al atoms, which are displaced during the $(\sqrt{3} \times \sqrt{3})R\,30° \rightarrow (2 \times 2)$ transition. Very recently, however, a combined total-energy calculation, LEED-IV, and SEXAFS study came to a slightly different model,[25,26] which will be discussed in light of the STM data below.

The outline of the paper is as follows. In Sec. II, we give a brief description of the experiment and of the coverage calibration by low-energy electron diffraction (LEED) and Auger-electron spectroscopy (AES). Section III describes the results obtained by STM together with LEED and AES observations. In III A the thermal stabilities of the $(\sqrt{3} \times \sqrt{3})R\,30°$ and (2×2) phases are characterized. It is found that these ordered phases represent the thermodynamically stable structures for $\Theta = 0.33$ and 0.5, respectively. In III B, we present STM results that characterize the nucleation and growth behavior of the lower coverage phase, and the substrate mass transport connected with its formation. The adsorption site of Na in this structure is deduced from STM data shown in III C. In this context, also, the closely related question of how Na atoms are imaged by the STM is addressed. The mobility found for Na atoms on substitutional sites, which differs substantially from that of ordinary adatoms is the topic of III D. The domain walls of the $(\sqrt{3} \times \sqrt{3})R\,30°$ structure, one of which may represent the nucleus for the (2×2) phase, and the transition to this higher coverage structure are characterized in III E. The last part of the results, III F, is devoted to the structure of the (2×2) phase. In Sec. IV, the results are discussed in comparison with the literature.

II. EXPERIMENT

The experiments were performed in a UHV chamber equipped with facilities for LEED and AES, an ion-gun and a home-built "pocked-size" STM.[27] Preparation of the Al(111) single-crystal sample consisted of repeated cycles of Ar^+ sputtering (500 eV, 3 $\mu A/cm^2$, 30 min, $T = 300$ K) followed by brief annealing to 800 K.[27,28] This treatment was continued until the surface concentration of the main contaminants, oxygen and carbon, had fallen below the AES detection limit (0.2% and 0.4% of a monolayer, respectively) and a sharp (1×1) LEED pattern was achieved. Sodium was evaporated from SAES getter sources (SAES getters SpA, Milano, Italy) at a rate of 1 ML in 100–200 s, with the Al(111) substrate held at 300 K. Prior to transferring the sample into the STM, its integral structure and coverage were characterized by LEED and AES. Auger-electron spectra recorded after the STM experiments revealed that the contamination level was still below 1% of a monolayer.

In situ preparation of the tungsten tip consisted of a high-field treatment (typically 300 V—tip positive—at a distance smaller 0.1 μm) in the STM in front of a clean Au foil which was used as a "dummy" sample. Subsequent voltage pulses of typically -5 to -7 V, applied to the sample during tunneling on Al(111), reproducibly lead to atomic resolution. This procedure and the resulting enhancement of lateral resolution were described in more detail in an earlier publication.[28] The fact that the tip becomes longer by 20–30 Å by this treatment has been interpreted either as material transfer from the sample to the tip or as a field-induced restructuring of the tip apex.[28] Since for a realistic theoretical treatment of the tip the chemical identity of the microtip is important, we mention the following observation: Voltage pulses applied while tunneling on a gold (111) surface resulted in

an identical tip change, i.e., a similar elongation correlated with an improvement of lateral resolution. The high-resolution state could be preserved when, after such a treatment, the Au(111) sample was replaced by the Al(111) crystal. However, the tips prepared in front of a Au(111) crystal turned out to be chemically much more inert than those prepared while tunneling on Al(111). They could be used over days without repeating the preparation procedure and turned out to be particularly well suited for experiments involving oxygen exposure.[27] It is, therefore, very plausible to assume that the actual tunneling microtip in the experiments shown here consists of a small cluster of sample material (either Al or Au) adsorbed at the tip apex.

The Na coverage was determined by AES ($E_p = 3$ kV, $I = 3$ μA), where the peak-to-peak ratio of the Na_{KLL} (990 eV) and the Al_{KVV} (1396 eV) Auger transitions were used. Calibration was achieved by comparison of LEED images and the corresponding AES signal. For AES intensity ratios of 0.16 and 0.25, respectively, the $(\sqrt{3} \times \sqrt{3})R\,30°$ and the (2×2) related LEED spots were most intense. For calibration it was assumed that these numbers correspond to the nominal coverages of the two structures of 0.33 and 0.50 ML, respectively.[23,24]

Scanning-tunneling-microscopy images shown here were recorded in the constant current mode. The sample bias voltage, the tunneling current, and the integral coverage as measured by AES are indicated in the figure captions. Images are unfiltered data to which a planar background subtraction has been applied. Scanning-tunneling-microscopy data are represented as top views with brighter gray levels corresponding to more elevated surface areas. In order to increase the contrast on individual terraces, we sometimes applied the full gray scale for each terrace separately. In these images atomic steps appear as black-white transitions.

III. RESULTS

A. Coverage regimes and thermal stability of the two ordered adsorption phases

In order to be able to relate the observations by STM of the atomic scale structures with the macroscopic Na coverages and with the structures averaged over larger areas, we performed experiments by LEED and AES. This is also the basis for the discussion of former results which were obtained by integral techniques.

For a sodium coverage of 0.14 ML the LEED pattern shows weak diffraction spots from the $(\sqrt{3} \times \sqrt{3})R\,30°$ phase which, henceforth, will be denoted as the $\sqrt{3}$ phase. At $\Theta = 0.32$, these spots have their maximum sharpness and are more intense than those of the Al(111) substrate. Increasing the Na coverage reduces the intensity of the $\sqrt{3}$ diffraction spots until they disappear completely at 0.5 ML. In the coverage range of $0.36 \le \Theta \le 0.50$ the $\sqrt{3}$ structure coexists with the higher coverage (2×2) phase. The (2×2) LEED pattern is (by definition) most perfectly developed at a coverage of half a monolayer. It becomes weaker with increasing Na coverage until it vanishes completely at 0.72 ML. At this coverage, also, the substrate lattice spots have almost

disappeared. The coverage ranges for which the $\sqrt{3}$ structure $(0.14 \le \Theta \le 0.50)$ and the (2×2) phase $(0.36 \le \Theta \le 0.72)$ are observed by LEED and the existence of a coexistence regime are in agreement with earlier experiments.[24] We, therefore, reproduce the remarkable finding that the sequence of ordered structures, $\sqrt{3}$ and (2×2) is reversed as compared to alkali adsorption on other hexagonally close-packed surfaces.[12] Also, we find no "ring structures" in the low coverage regime, which normally precede the lowest coverage ordered structures in other systems,[12] again in agreement with earlier findings. These observations demonstrate the peculiarity of the Na/Al(111) system. From the STM data presented below, we will deduce a detailed microscopic scenario that can account for these findings.

Annealing experiments gained information on the thermal stability of the respective phases. Annealing the sodium-saturated surface $(\Theta \approx 1$ ML$)$ at 370 K for 1 min leads to the appearance of sharp (2×2) LEED spots, together with a coverage decrease to $\Theta = 0.5$, as detected by AES. When the sample is kept at this temperature for a longer time, the (2×2) phase transforms into the $\sqrt{3}$ structure. This structure is found to be more stable, i.e., both the coverage of 0.33 ML as well as the sharp $\sqrt{3}$ LEED pattern do not change upon further annealing at 370 K. Only at higher temperatures, between 450 and 500 K, the $\sqrt{3}$ structure is converted into the clean (1×1) surface. The removal of adsorbed sodium from the surface most likely proceeds via desorption rather than via diffusion into the bulk under these conditions. The latter process is unfavorable because of the extremely low solubility of Na in Al. The observation that desorption of sodium adsorbed in the (2×2) structure sets in at lower temperatures compared to that from the $\sqrt{3}$ structure agrees perfectly with results of recent TDS experiments where two peaks corresponding to desorption from these phases were found at 433 and 505 K, respectively.[29]

B. Nucleation and growth of the $(\sqrt{3} \times \sqrt{3})R\,30°$ structure

In this section, we present STM observations on surfaces in the low coverage regime with Na coverages below that of a fully developed $\sqrt{3}$ layer $(\Theta_{Na} = 0.33)$. These data, in particular those on the distribution of small amounts of Na on the surface, yield the important information about the formation mechanism of the $\sqrt{3}$ phase and thereby also about the interactions between the adsorbed Na atoms.

Figures 1(a) and 1(b) show STM images of the Al(111) surface covered with 0.12 and 0.20 ML of sodium, respectively. These images show a sequence of flat terraces, separated by monolayer steps of 2.33-Å height. For representation the images have been tilted in such a way that the terraces appear brighter close to the descending steps and darker in the vicinity of the ascending ones. On the terraces we find bright patches, indicating that areas with a geometric or electronic structure different from that of the surrounding substrate, have formed. Scanning-tunneling-microscopy images recorded with lower tunnel resistance resolve a $\sqrt{3}$ structure in the islands (see the next chapter). Hence, these features are identified as islands of the $\sqrt{3}$ Na phase. This is corroborated by the

LEED pattern of this surface which exhibits clear $\sqrt{3}$ spots. The local Na coverage in these islands was derived from the ratio of the integral coverage of the surface shown in Fig. 1(b), 0.20 ML as measured by AES, and the fraction of 0.60 of the surface that is covered by these islands (the latter value is obtained from the height distribution in that image). On this basis, we find a local Na coverage of 0.33 ML, i.e., exactly the nominal value expected for the $\sqrt{3}$ phase. We, therefore, conclude that sodium forms islands of the $\sqrt{3}$ phase for total (i.e., integral) coverages below 0.33 ML. In fact, island formation is already found in STM images for rather low coverages, e.g., at 0.06 ML of Na.

The tendency towards island formation points to attractive interactions between the Na adsorption complexes which must overcompensate the dipole-dipole repulsion between these entities that usually dominates in alkali adsorption systems. This attraction favors island formation instead of the two-dimensional (2D) gas of alkali adatoms expected on close-packed metal surfaces in the low coverage regime. More detailed inspection reveals that nucleation occurs preferentially at the upper terrace side of steps. In Fig. 1(a) the larger terrace on the right bottom is almost free of the $\sqrt{3}$ phase, only the region near the step is covered by it. In contrast, the narrow terraces in the upper part of the image exhibit a relatively high $\sqrt{3}$ coverage. In Fig. 1(b) the majority of the $\sqrt{3}$ patches is connected to the steps, from the upper terrace side, whereas none of them is attached to them from the lower terrace side. In addition, those patches, which are found on central regions of terraces, are smaller than those connected to steps. These results point to a mechanism involving a heterogeneous nucleation process with preferential nucleation at steps, more precisely on the upper terrace side of steps, and a higher growth rate of the nuclei created at the steps as compared to those originating from homogeneous nucleation on the terraces. Both, island formation and the structure selective nucleation and growth behavior of the $\sqrt{3}$ phase point to a geometry of the $\sqrt{3}$ structure distinctively different from that of an adsorbed alkali layer on an unreconstructed hexagonally close-packed substrate.

The STM image in Fig. 2 shows an area of the surface with an integral Na coverage of 0.29 ML. One of the terraces extends over almost 2000 Å. On this terrace, there are still extended regions of the clean substrate (dark) between the $\sqrt{3}$ islands (bright), whereas the smaller terraces are almost completely covered by the alkali-metal layer. This again is due to a faster 2D growth of islands at upper terrace edges. Figure 2, however, shows additional features which were not seen on the two preceding images. Some terraces carry small, brighter islands with a height difference of a substrate step. Also, one (sub-
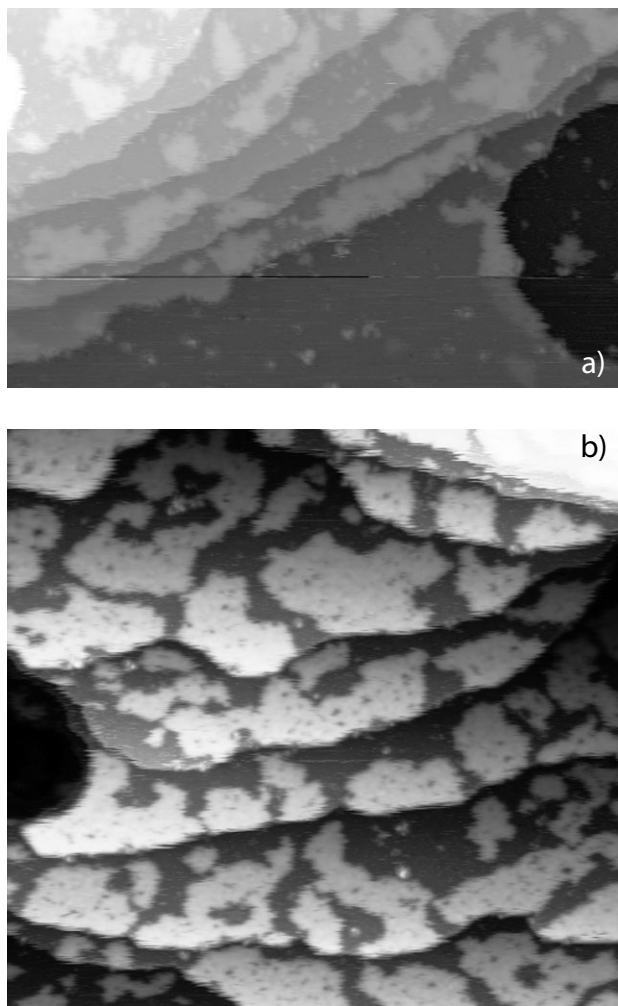

FIG. 1. Scanning-tunneling-microscopy images of a low coverage Na covered Al(111) surface. The bright patches represent Na islands with a $(\sqrt{3} \times \sqrt{3})R\,30°$ structure. (a) shows preferred nucleation at steps, (b) the increased growth of islands connected to steps [(a) $\Theta = 0.12$, 800×400 Å^2; (b) $\Theta = 0.20$, 1000×1000 Å^2, (a) and (b) $I_t = 0.1$ nA, $V_t = -2.0$ V].
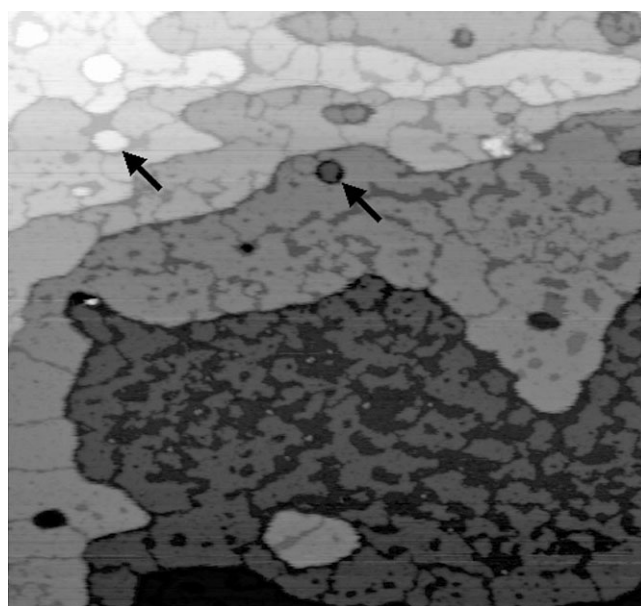

FIG. 2. Scanning-tunneling-microscopy image of a higher coverage Na coverage Al(111) surface, illustrating that Na adsorption leads to mass transport of substrate material, indicated by islands and holes on terraces. One of each is marked by an arrow [$\Theta = 0.29$, sharp $(\sqrt{3} \times \sqrt{3})R\,30°$ LEED pattern, $I_t = 0.1$ nA, $V_t = -2.0$ V, 2000×2000 Å^2].

strate) layer-deep holes are found in Fig. 2 (see arrows in the upper part of the image). Both, the protrusions and the holes are partly Na covered as is the rest of the surface. Since these features are usually not found on the clean surface, they must originate from a restructuring of the substrate induced by Na adsorption at $T = 300$ K. We will discuss below why these features are less abundant than expected and even completely absent on some areas. Summarizing this part, we find that the $\sqrt{3}$ phase grows via island formation, that steps represent areas of preferred nucleation or growth, and that there are indications of a larger scale rearrangement of the aluminum substrate induced by the alkali-metal adsorbate.

C. STM imaging and adsorption site of Na in the $\sqrt{3}$ structure

In the STM images presented above, the $\sqrt{3}$ islands appear flat and between 1 and 3 Å higher than the uncovered substrate areas. The exact height difference varies strongly with the tip condition, it is 3.2 Å for Fig. 1(b) and 1.2 Å for Fig. 2 (both recorded at $R_{gap} = 2 \times 10^{10}$ Ω). For similar tip conditions, however, the apparent height of the $\sqrt{3}$ islands varied reproducible with tunnel current. It becomes smaller when the tip approaches the surface. This can be rationalized in terms of a locally reduced barrier height above the Na-covered areas, as will be discussed in more detail in IV B. A further effect of the decreasing distance between tip and sample is that the atomic structure of the Na islands can be resolved (see Fig. 3). The islands reveal a hexagonal pattern of protrusions with a periodicity of 5.0 Å, which is exactly $\sqrt{3}$ times the crystallographic spacing between the Al substrate atoms. The close-packed directions of this structure are rotated by 30° with respect to those of the Al(111) surface, as can be seen from the two black lines at the top of Fig. 3 where both lattices, that of the adsorbate and that of the substrate, are resolved. Hence the periodic corrugation in the islands is identified as the atomic structure of the $\sqrt{3}$ phase formed by Na on Al(111).

Next, we try to get more information on the lateral position of the sodium atoms in the $\sqrt{3}$ phase with respect to the substrate. This is a very direct test of the validity of the structure model proposed in the SEXAFS study.[14] If that model were correct, the sodium atoms should be located at the same positions as the aluminum atoms of the surrounding terrace. First, however, we have to make sure that the protrusions seen in the STM topographs for sufficiently large R_{gap} can in fact be identified with the adsorbed Na atoms. Based on former STM studies[17,30−33] and, also, from the contrast inversion for low R_{gap} in the present system (see below), this cannot be assumed a priori. This assignment is possible on the basis of symmetry arguments. In the $\sqrt{3}$ structure, the adsorbate atoms form a hexagonal lattice with a lattice constant d_{nn}, which is $\sqrt{3}$ times larger than that of the substrate. In contrast, the hollows in that structure form a honeycomb lattice with the next-nearest-neighbor distance d_{nn} of the substrate. Based on this argument the hexagonally arranged protrusions in Fig. 3 are identified as the Na atoms. The finding that the Na atoms in the

$\sqrt{3}$ phase can be resolved in STM measurements is remarkable by itself. In STM studies of Na adsorption on Au(111) (Ref. 30) no localized atomic features were seen as long as the substrate did not reconstruct. This was attributed to the high mobility of *overlayer* alkali-metal atoms which, in turn, means that the situation has to be considerably different for Na on Al(111).

Imaging of the $\sqrt{3}$ structure is found to be inverted if the STM tip is approached closer to the surface. This effect is demonstrated in Fig. 4 which shows a $\sqrt{3}$ island and a part of the clean substrate. In the center of the image, the Na atoms are imaged as protrusions similar to Fig. 3. In the upper and the lower part, the Na atoms are imaged as hexagonally arranged depressions. This was achieved by reducing the tunneling resistance and, therefore, the distance between tip and sample for the upper and the lower part of the image. That these changes indeed result from a controlled change in tunnel gap and not from an uncontrolled change in the tip is supported by both, the reversible nature of the change in imaging behavior, and by the fact that minima and maxima in the two differently imaged areas are exactly lined up (see black line in Fig. 4).
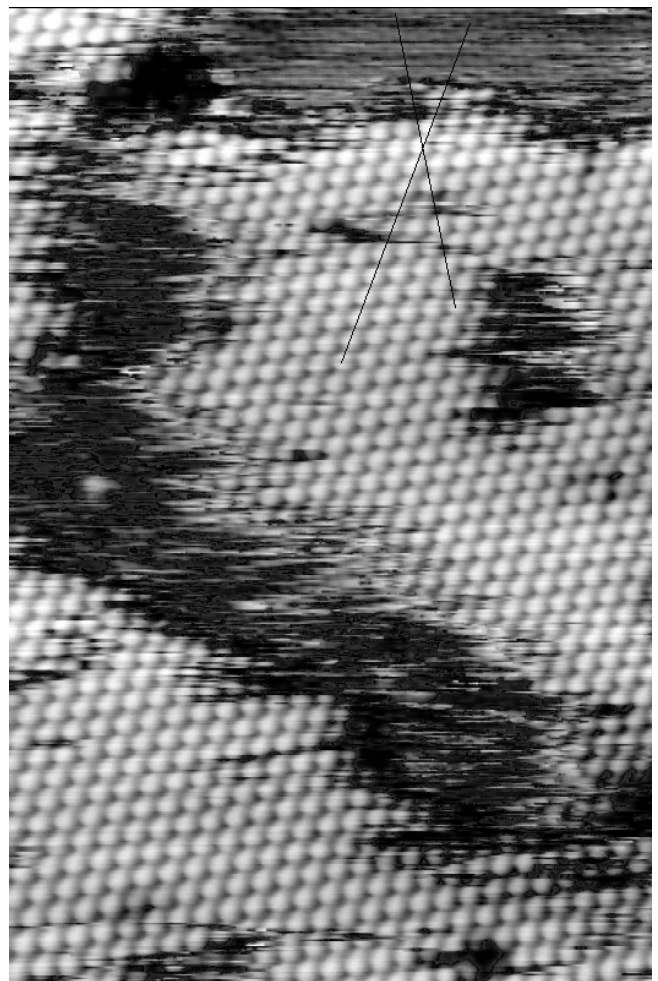

FIG. 3. Scanning-tunneling-microscopy image showing the atomic structure of the $(\sqrt{3} \times \sqrt{3})R\,30°$ phase formed by Na on Al(111) at $T = 300$ K. Hexagonal arranged protrusions are identified as Na atoms. Dark areas represent clean substrate $(\Theta = 0.24, I_t = 10$ nA, $V_t = -1.0$ V, 123×177 Å^2).

The lateral adsorption site of Na in the $\sqrt{3}$ islands can be determined from the registry of atoms in Fig. 5, showing a $\sqrt{3}$ structure on an Al(111) terrace. Note that in this case the $\sqrt{3}$ is imaged in the inverted mode, with the Na atoms appearing as hexagonally arranged depletions, embedded in a protruding area formed by the hollows of the $\sqrt{3}$ structure. In addition to the $\sqrt{3}$ structure, also, the close-packed rows of the Al substrate atoms as well as contaminations such as adsorbed carbon atoms are resolved.[27,34] The sodium atoms lie exactly on lines drawn through the bright lines of the substrate marking the close-packed rows of substrate. Hence, the depressions in the STM contour representing the Na atoms are exactly in phase with the close-packed rows of Al atoms. On the other hand, the carbon defect atom (at the coordinates $x \approx 20$ Å, $y \approx 60$ Å in the topograph) is clearly out of phase with these rows as expected for its hcp-adsorption site.[34] This means that the lateral position of

FIG. 5. Scanning-tunneling-microscopy topograph illustrating that Na atoms in the $\sqrt{3}$ islands, imaged as depletions, are located in phase with the Au(111) surface atoms ($\Theta = 0.15$, $I_t = 32$ nA, $V_t = -0.5$ V, 103×113 Å^2).

Na in the $\sqrt{3}$ structure coincides with the positions of first layer Al atoms, pointing to an on-top or substitutional adsorption site.

The adsorption characteristics derived from STM observations, namely, the preferred nucleation and growth at descending steps, the substrate mass transport, the net attractive interaction leading to island formation, are highly untypical for alkali-metal adsorption on a close-packed metal surface. In combination, they can only be described by a model including a reconstruction of the surface. Together with the lateral position of Na, identified as in phase with the Al surface lattice, these STM observations point to a replacement of Al atoms by the adsorbed sodium and, thus, to a substitutional adsorption geometry. The present STM data, therefore, confirm the substitutional adsorption site, first proposed on the basis of SEXAFS data and total-energy calculations.[14,18]

D. Mobility

In cases where adsorbates travel across a surface at a speed comparable to that for image acquisition, STM measurements can provide quantitative information about surface diffusion constants. This is usually not possible for alkali-metal atoms adsorbed on flat metal surfaces, since hopping rates are by orders of magnitudes too high at room temperature. On the other hand, we have shown above that the Na atoms inside the $\sqrt{3}$ islands are immobile which renders it impossible to study adsorbate motion there. However, there is some motion of Na atoms at the perimeter of the islands and between the islands. For instance, the dark area representing the clean substrate between the two Na islands in Fig. 3 is dis-
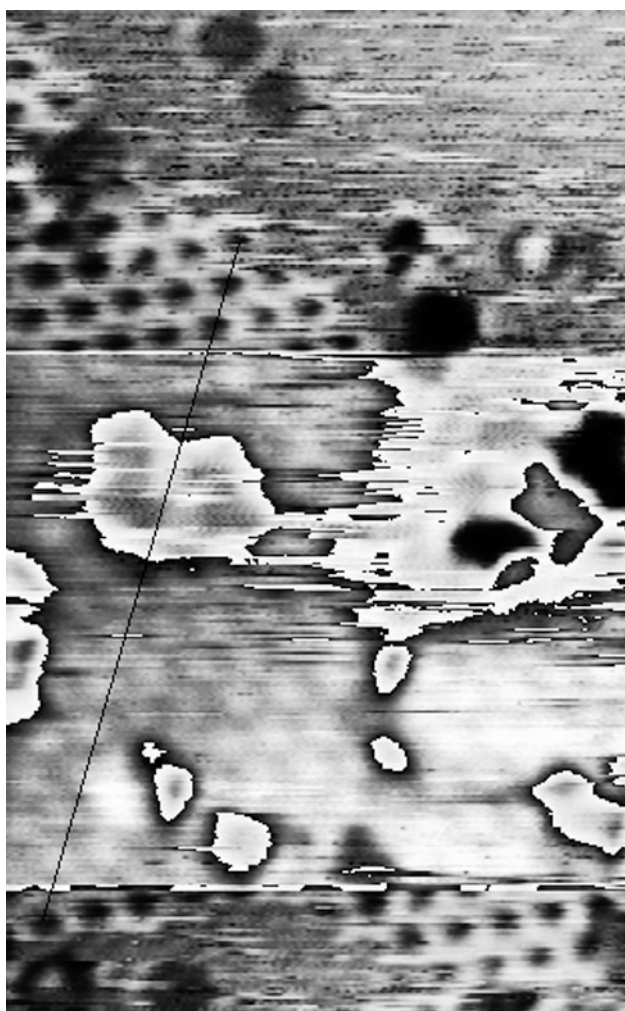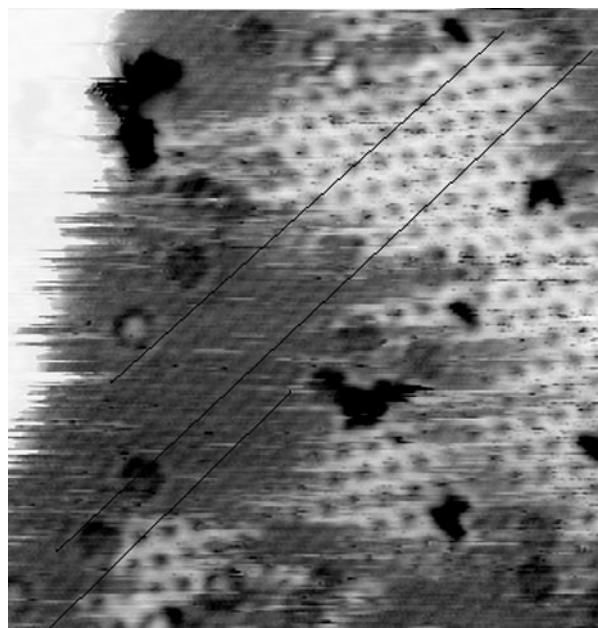

FIG. 4. Scanning-tunneling-microscopy image of a medium coverage Na covered surface, where a $\sqrt{3}$ island is imaged under different tunneling conditions. The upper and lower part shows the inverted imaging of the $\sqrt{3}$ structure, induced by approaching the tip further to the surface. Na atoms appear as depletions in these STM images ($\Theta = 0.14$, $I_t = 32$ nA, $V_t = -0.4$ V in the upper and lower part, $V_t = -0.6$ V in the middle, 62×100 Å^2).

turbed by frequent vertical jumps of the tip by 0.5 Å, which is exactly the level of the $\sqrt{3}$ islands. These jumps appear as white stripes. At the same time, the borders of the islands are not smooth but appear frizzy. Furthermore, some of the sodium atoms located at the island perimeter are imaged only partly which indicates that they have moved during the time it took to image one Na atom. We interpret these observations as the result of a motion of Na on the time scale of the STM experiment. Similar behavior is reflected by the fringes in the step edge on the left-hand side of Fig. 5, which represents a step between the $\sqrt{3}$ covered upper terrace and a clean substrate lower terrace.

A quantitative analysis of the surface mobility was performed by following the evolution of island sizes with time. This is shown by Figs. 6(b)–6(d), where topographs of a partly Na-covered surface area have been recorded in time intervals of 125 s. Figure 6(a) shows an overview over a larger area; Figs. 6(b)–6(d) a detail which was taken on the left-hand terrace in Fig. 6(a). First, it is obvious that the shapes of the three islands changed with time. (The dark round features indicating immobile contaminants may serve as fix points.) Second, a fourth small island consisting of four Na atoms developed in Fig. 6(c) [compare the image centers of Figs. 6(b) and 6(c)]. Furthermore, the size of the three larger islands changes with time. The upper island, e.g., consists of 60-Na atoms in Fig. 6(b), while 125 s later it has only 38 atoms [Fig. 6(c)] and 42 atoms in Fig. 6(d). At the same time, the island at the lower part of Figs. 6(b)–6(d) has increased in size. Hence there is a continuous redistribution of Na atoms on the surface, either by exchange between existing islands, or by creation of islands of the $\sqrt{3}$ phase. The integral Na coverage, however, is constant in course of these local fluctuations (see the above LEED results about the thermal stability of the $\sqrt{3}$ phase).

In order to evaluate the effective diffusion constant from these observations, we assume that the 22 atoms which are removed from the upper island in Figs. 6(b) must at least have traveled an area of half of the image, i.e., 140×140 Å^2 during the time interval of 125 s between recording Figs. 6(b) and 6(c). The island initially consisted of 60 atoms, 22 of which 22 have migrated away. From this we obtain a lower limit for their diffusion constant of $D \geq (140$ Å$)^2/125$ s $\times$ 22/60 $= 6 \times 10^{-15}$ cm^2/s at the sample temperature of 300 K. This value is a lower limit for the diffusion constant also for a second reason. It includes the release of atoms from the edges of the islands which because of the attractive interactions within the islands presumably is the rate limiting step. Hence, the actual diffusion constant for the adsorbates already detached from the islands must be higher than the number estimated.

Actually, the diffusion constant for this latter process, i.e., for independent-particle motion, can be derived from our data as well. The white stripes on the substrate between the sodium islands in Figs. 3 and 6 can be associated with Na atoms migrating between neighboring islands. These stripes are not observed on the clean surface and their height of 0.5 Å in Fig. 6 corresponds exactly to the apparent height of sodium in the $\sqrt{3}$ islands with respect

to the substrate. The fact that all of the stripes in Fig. 6 are only one scan line wide means that the sodium atoms have moved in the time interval between two successive scan lines of 0.25 s. As a result, there is no correlation between the location of the stripes from line to line. From the observation that the stripes all have approximately the same length [see Fig. 6(a)], it can be concluded that the migration speed must be smaller than the scanning speed in the fast scan direction. Otherwise, one would have observed longer and shorter stripes caused by atoms moving along and against the scan direction and the diffusion speed can be extracted from the width of the distribution function for the stripe length. In our case, this distribution function is rather narrow [see Fig. 6(a)], which means that normally the atoms do not jump away while the tip moves across them. For the scanning speed of 3 Å/ms used here, this gives an upper limit for the hopping frequency of 1×10^3 s^{-1} and of 2×10^{-13} cm^2/s for the diffusion rate. As a result, we have calculated D by two independent methods. The actual value for the diffusion constant D for the diffusion of (substitutional) Na on Al(111) at room temperature must lie in a relatively narrow range between 6×10^{-15} cm^2/s and 2×10^{-13} cm^2/s.

The similar apparent height of these mobile Na species and the Na adsorbed in the $\sqrt{3}$ islands points to similar adsorption sites in both cases (Na adsorbed in an overlayer fcc (on-top) position, with the bond length determined by SEXAFS (Ref. 14) is located 1.2 Å (1.6 Å) higher than the substitutional Na atoms and would be expected to show up differently in STM images). Hence diffusion proceeds by migration of a substitutional Na atom within the topmost Al layer. Further details of the migration process, in particular the nature of the transition state, are discussed in Sec. IV. Independent of this, it is clear that its activation energy must be significantly higher than that for the migration of Na adatoms on the flat (1×1) Al(111) surface. For the latter process the activation barrier has been calculated to $E_m < 30$ meV.[35] Similarly, high mobilities are usually observed when alkali-metal atoms are adsorbed on a close-packed metal surface. In STM images this highly mobile 2D gas appears transparent, as, e.g., observed for Na adsorbed on Au(111) for coverages up to 0.2 ML.[30] Due to the fact that even single Na atoms on Al(111) create and maintain a local reconstruction at 300 K, they have a much lower mobility on this surface compared to an overlayer alkali atom. It can, of course, not be excluded that at the same time further Na atoms are adsorbed on ordinary surface sites which then would be highly mobile and transparent to the STM. However, from comparison of AES data and STM coverages this latter species can only account for a very small fraction of the adsorbed Na, whereas the majority resides on substitutional positions and, therefore, reveals a relatively low mobility. A highly mobile alkali-metal adlayer is expected for Na/Al(111) only for low temperatures where the activation barrier for reconstruction cannot be overcome [see, e.g., K/Al(111) (Ref. 36)]. In summary, an estimate for the surface diffusion constant of substitutional Na atoms on Al(111) at 300 K can be given, and it is found that this traveling species is
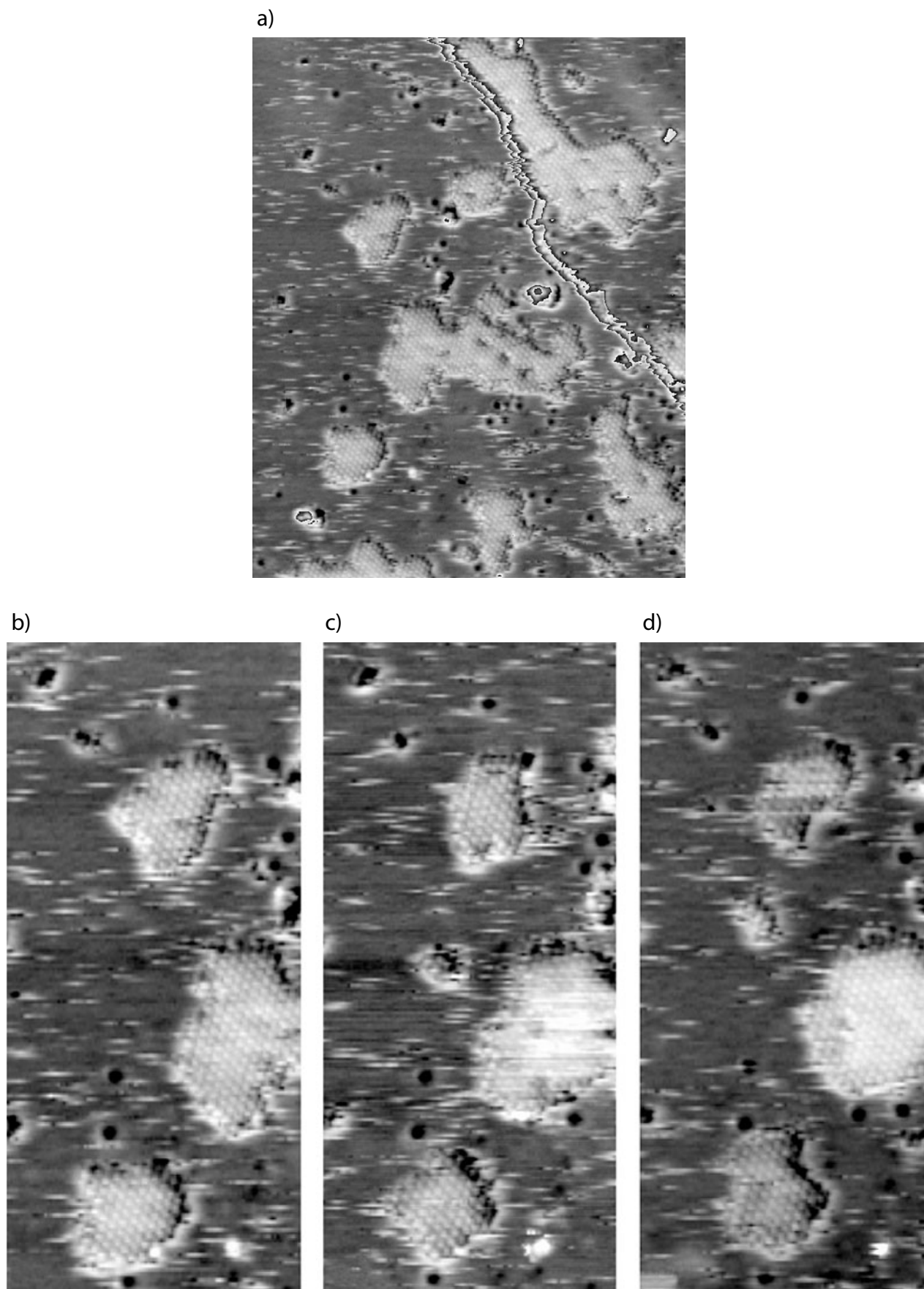
FIG. 6. Scanning-tunneling-microscopy images showing the evolution of the same area of the partly covered Al(111) surface with time. Images (b), (c), and (d) have been sequentially recorded each 125 s, (a) shows an overview. The mobility of Na is obvious from white stripes between the islands, representing a Na atom temporarily located under the tip, and from fluctuations of island sizes and shapes with time [$\Theta = 0.12$, $I_t = 0.1$ nA, $V_t = -2.0$ V; (a) 364×460 Å^2; (b)–(d) 140×308 Å^2].

similar to that localized in the $\sqrt{3}$ islands, i.e., a substitutional Na atom in a substrate vacancy.

E. Domain walls and coexistence of $(\sqrt{3} \times \sqrt{3})R\,30°$ and (2×2) structure

In this paragraph, we present data about the defect structure that is formed upon completion of the $\sqrt{3}$ layer and about the nucleation of the (2×2) phase. The $\sqrt{3}$ structure can exist in three transitional domains, displaced from each other by one substrate unit vector. For Na coverages below completion of the $\sqrt{3}$ structure, domain boundaries appear dark in STM images. This points to a reduced local coverage ("light walls"). As demonstrated in Fig. 7, which shows two islands of different domain types, these "light walls" are areas of high mobility, with a continuous exchange of Na atoms between adjacent domains. In spite of this high degree of mobility it was never observed that a domain wall is removed, which would require the transformation of a complete domain. The density of domain walls is observed to remain constant over hours even if their position is fluctuating. Therefore, the ordered alkali-metal structure at 300 K, at coverages slightly below 0.33 ML, is always characterized by a certain density of domain boundaries.

When the Al(111) surface is covered by a complete $\sqrt{3}$ layer, also, the step structure is affected. This is demonstrated in Fig. 8(a), which shows that on this surface the steps are straight over distances of the order of 100 Å. The step directions are rotated by 60° against each other.
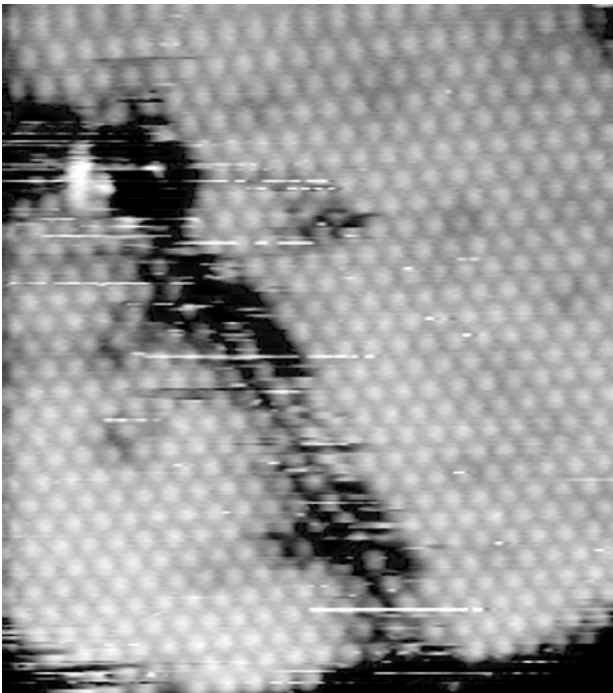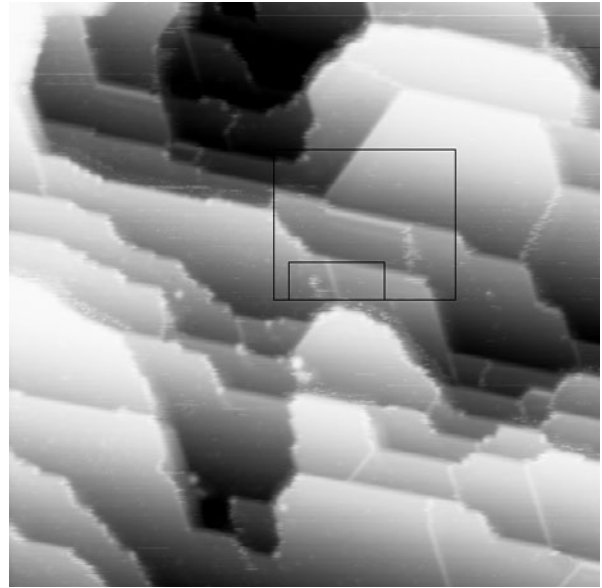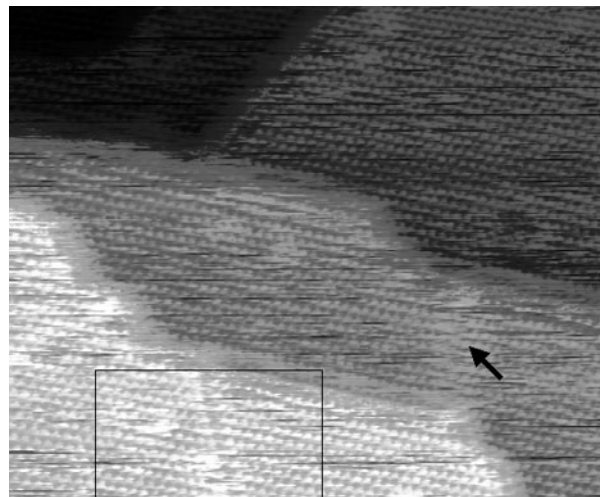

FIG. 7. Scanning-tunneling-microscopy topograph of two $\sqrt{3}$ islands which are separated by a "light wall." The streaks are due to fast exchange of atoms between the two islands $(\Theta = 0.30, I_t = 3.0 \text{ nA}, V_t = -1.2 \text{ V}, 110 \times 124 \text{ Å}^2)$.
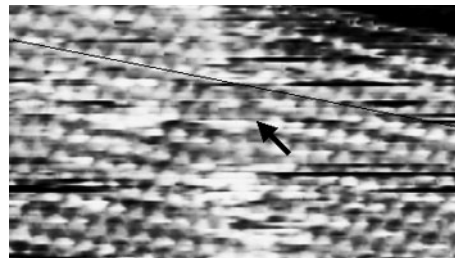
a)

b)

c)

FIG. 8. Scanning-tunneling-microscopy images of the surface covered with a complete $(\sqrt{3} \times \sqrt{3})R\,30°$ Na monolayer, (a) overview, (b) and (c) details recorded at the rectangles marked in (a) which resolve the atomic structure of the terraces. The surface shows step alignment; furthermore, domain boundaries change into "heavy" walls, imaged as bright stripes in (a) $[\Theta = 0.33, \text{ sharp } (\sqrt{3} \times \sqrt{3})R\,30° \text{ LEED pattern, (a) } I_t = 3.0 \text{ nA}, V_t = -1.2 \text{ V}, 870 \times 870 \text{ Å}; \text{ (b) } I_t = 3.0 \text{ nA}, V_t = -0.5 \text{ V}, 260 \times 240 \text{ Å}^2; \text{ (c) detail from (b) } 90 \times 55 \text{ Å}^2]$.
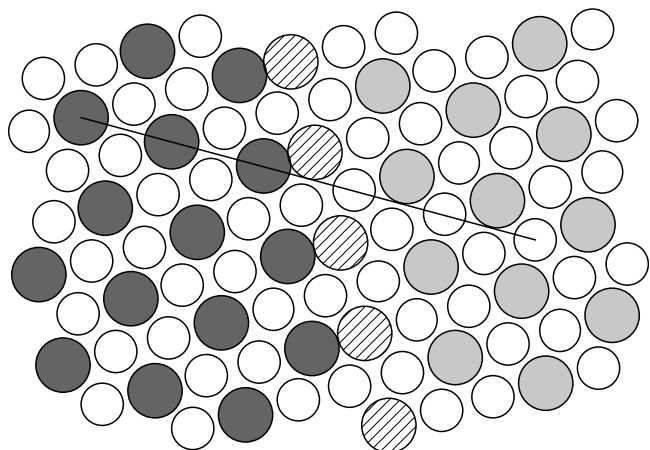
FIG. 9. Structural model (top view) of the two $\sqrt{3}$ domains imaged in Fig. 8(c). Na atoms are sketched as filled circles, Al atoms with their smaller radius as smaller open circles, Na atoms introduced between the domains are represented as hatched circles, they presumably fluctuate between sites located on nearest-neighbor positions to the left and right domain.

The close-up [Fig. 8(b)] taken on the marked area reveals that these preferred step orientations are the close-packed $[11\bar{2}]$ directions of the $\sqrt{3}$ structure. This step realignment must include a considerable rearrangement of the reconstructed Na-Al terraces, since on the clean surface steps are mostly randomly oriented, with only short sections oriented along $[1\bar{1}0]$, but never along the $[11\bar{2}]$ direction. This random step orientation is maintained up to a sodium coverage of 0.29 (Fig. 2), the steps become aligned only at coverages where the $\sqrt{3}$ layer is completed. This indicates that the driving force for the observed step alignment is connected with the filling up of the remaining substrate areas along the ascending steps. On the other hand, the step alignment is evidence for a more rigid surface layer compared to the submonolayer region, i.e., the $\sqrt{3}$ layer tends to adopt shapes with better defined borders.

In the same images, in Figs. 8(a), 8(b), we find a structural element not observed so far, namely, bright stripes running over the terraces. These stripes also represent domain walls. This becomes more obvious from inspection of the enlarged image in Fig. 8(c),
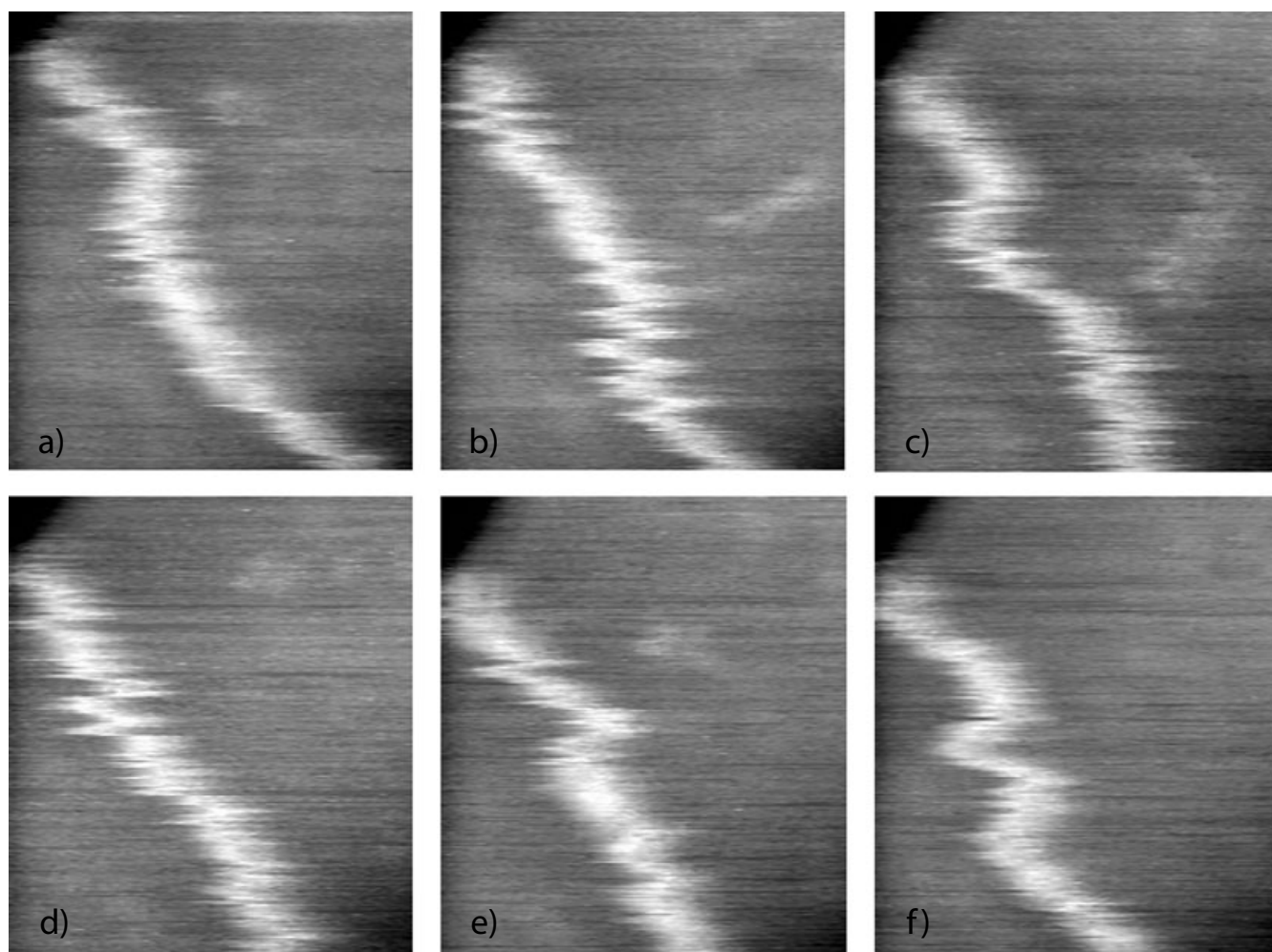

FIG. 10. Series of STM images illustrating the mobility of those "heavy" walls, which are not oriented along the $\sqrt{3}$ symmetry direction; (a)–(h) successive images taken every 8 s [$\Theta = 0.35$, LEED $(\sqrt{3} \times \sqrt{3})R\,30°$, $I_t = 3.0$ nA, $V_t = -0.7$ V, 118×116 Å^2].

representing the area of the smaller rectangle marked in Fig. 8(a). The Na rows on the left-hand side are shifted by $\frac{1}{3}$ of their distance with respect to those from the right domain. Contrary to the situation at $\Theta < 0.33$, the domain walls are now imaged as protruding stripes [$\Delta z = 0.5$ Å in Fig. 8(a)]. It is plausible to associate them with areas with a locally higher sodium coverage. The domain boundary itself is again frizzy, indicating a considerable mobility of the Na atoms in this area. At those positions where Na atoms at the domain boundary remain at their sites sufficiently long, it is seen that they are at positions in phase with the right domain and on Al nearest-neighbor distance to Na atoms of the left domain [one of them is marked with an arrow in Fig. 8(c)]. This is illustrated in the sketch in Fig. 9. The atomic structure of the domain boundaries at $\Theta = 0.33$ can be described by an extra row of atoms (marked dashed in Fig. 9) introduced between adjacent domains. Because of the locally increased coverage, this type of domain boundaries is denoted as "heavy walls."

The position of the [$11\bar{2}$]-oriented domain wall in Fig. 8(c) does not change with time. This type of domain boundary, therefore, appears as a straight bright line in the overview image in Fig. 8(a). In addition to these straight lines, Fig. 8(a) also reveals domain boundaries appearing in a zigzag manner. One of them is included in the detail in Fig. 8(b) (see arrow). The sequence of STM images reproduced in Figs. 10 illustrates the evolution of this second type of domain boundary with time. Successive images were recorded in intervals of 8 s, they demonstrate that the domain wall changes its position by up to 20 Å in subsequent images which leads to the observed zigzag shape. The zigzag-type domain walls must be intrinsically different from the oriented ones, because even though there is a high mobility they do not orient along the [$11\bar{2}$] direction. With further increase of the Na coverage this type of domain boundaries becomes more frequent as compared to the [$11\bar{2}$]-oriented ones, suggesting that the local Na coverage in these zigzag domain walls is even higher than that in the [$11\bar{2}$]-oriented type.

Increasing the Na coverage above 0.33 ML leads to the formation of small islands of the (2×2) phase. The STM image reproduced in Fig. 11(a) shows such a small island on the upper part of the image, coexisting with the completed $\sqrt{3}$ phase which covers most of the terraces. The island is characterized by a different internal structure and a slightly protruding borderline, separating it from the lower-lying $\sqrt{3}$ phase. The line scan in Fig. 11(b), taken at the upper part of Fig. 11(a), shows that the (2×2) island is imaged 1.2 Å higher than the adjacent $\sqrt{3}$ layer; the distance between subsequent $\sqrt{3}$ layers is equivalent to the Al(111) layer distance of 2.3 Å. The formation of the (2×2) phase starts always at the ascending step edges of the $\sqrt{3}$-structured Na-Al terraces.

Upon further increasing the Na coverage, an increasing part of the surface converts from the $\sqrt{3}$ into the (2×2) phase. An example with 0.40-ML Na is shown in Figs. 12(a) and 12(b). In the close-up, Fig. 12(b) the atomic structure is resolved for both phases simultaneously. As expected, the close-packed directions of the two structures differ by 30° (see the two lines marking the

close-packed directions of each structure). From their hexagonal structure with a lattice constant of 4.9 Å the areas on the left-hand side and lower right-hand side of the image are identified as $\sqrt{3}$ phase. On the remaining areas which equally exhibit a hexagonal corrugation, the lattice constant is larger (5.7 Å) and the lattice is rotated by 30° with respect to that of the $\sqrt{3}$ areas. This structure, which also appears higher by 1.2 Å than the $\sqrt{3}$ phase in the STM images, is, therefore, identified as the (2×2) phase. Its atomic structure is resolved with a higher corrugation amplitude than that of the $\sqrt{3}$ phase.

The bottom of Fig. 12(b) overlaps with the upper marked part of the overview reproduced in Fig. 12(a). This allows us to unambiguously identify the "brighter" areas in Figs. 12(a) as the (2×2) phase and the darker areas adjacent to the left and right, which are lower by 1.2 Å, as $\sqrt{3}$ structure. In Fig. 12(a) (2×2) areas are labeled, the areas with differing height—respectively, gray levels in between—correspond to $\sqrt{3}$-structured areas. Of further help in this assignment is the characteristic protruding line bordering (2×2) structured areas at their descending steps, which is not found for $\sqrt{3}$ areas. As the lower coverage structure does, also the (2×2) phase exhibits domain boundaries, they are imaged as bright stripes in Fig. 12(a). Figure 12(b) shows a (2×2) domain
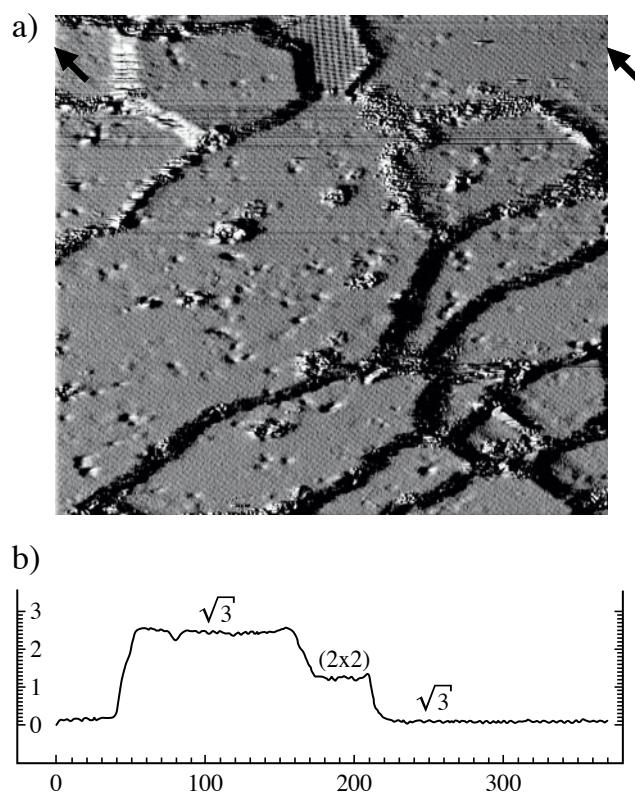

a)

b)

FIG. 11. Scanning-tunneling-microscopy image of an island of the (2×2) phase with a local coverage of 0.5, formed by Na when increasing the coverage above 0.33. The island is characterized by a pronounced vertical corrugation resolved here, a protruding borderline and an apparent height of 1.2 Å [line scan (b)] above the adjacent $\sqrt{3}$ structured terrace [$\Theta = 0.35$, LEED ($\sqrt{3}\times\sqrt{3})R30°$, $I_t = 10$ nA, $V_t = -0.6$ V, 370×330 Å, representation by illumination from the left].
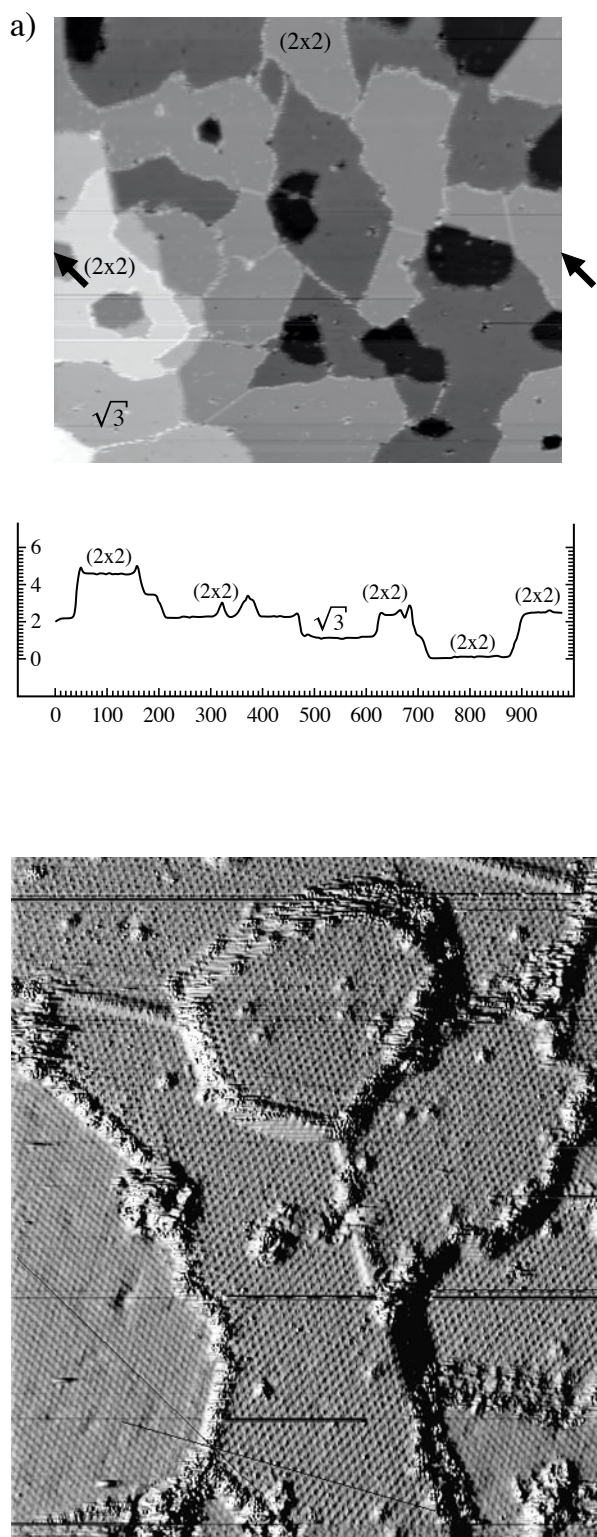
a)

FIG. 12. Scanning-tunneling-microscopy images recorded on a surface with (2×2) and $\sqrt{3}$ phase coexistent. (a) Overview image, (b) higher resolution image of the area marked by a rectangle in (a), resolving the atomic structure of both phases. The overlap with the overview in (a) allows us to assign the structure to the areas imaged as different height levels, the line scan in (a) shows the identification of (2×2) and $\sqrt{3}$ areas by their imaging height [$\Theta = 0.40$, LEED ($\sqrt{3} \times \sqrt{3}$)R30° coexistent with (2×2), (a) $I_t = 13$ nA, $V_t = -1.0$ V, 980×900 Å^2; (b) $I_t = 34$ nA, $V_t = -0.7$ V, 362×422 Å^2].

boundary at the upper left corner where close-packed rows are shifted by one-half of their distance.

It is interesting to note that all of the boundaries between $\sqrt{3}$ domains in Fig. 12(a) are of the zigzag type. Their increasing abundance as well as their increased imaging height with respect to the "heavy" walls which are straight [they are imaged with $\Delta z = 1.2$ Å, similar to the level of the (2×2) structure in Fig. 12(a)] found for these "heavy" domain walls with increasing Na coverage suggests that the (2×2) phase evolves from these areas which exhibit a locally increased Na coverage.

In conclusion, the data show that upon reaching the ideal coverage of 0.33 for the $\sqrt{3}$ phase, the Na-Al layer becomes more stable, i.e., fluctuations with substitutional Na atoms exchanging between neighboring antiphase domains become much less pronounced than at lower coverages. Two types of domain walls are seen, "light" and "heavy" ones which differ by the concentration of Na adsorbates located in them. The latter presumably represent the nucleus for the (2×2) phase.

F. The (2×2) unit cell

The STM data allow us, also, to draw conclusions on the structure of the (2×2) phase, which has so far been much more uncertain than that of the $\sqrt{3}$ phase. The STM images presented in Figs. 13 show that the (2×2) structured areas are imaged as a simple hexagonal pattern with one protrusion per unit cell and a nearest-neighbor distance between the protrusions of 5.7 Å, which is two times that of the underlying substrate. The bright stripes running in vertical direction are domain boundaries of the (2×2) structure. Figure 13(a) shows two of the four possible domains, in Fig. 13(b) there are three.

It is evident from the coverage of 0.5 ML that the (2×2) unit cell must contain two Na atoms. From the observation of one protrusion per unit cell a simple first guess for a (2×2) structure model with two Na atoms on substitutional sites, in analogy to the $\sqrt{3}$ phase, can already be ruled out. (In such a structure the distance between the substitutional Na atoms would be unreasonably small compared with the sodium bulk value of 3.66 Å. Also equal imaging of these two electronically and geometrically equal Na atoms would have to be expected, which is clearly not observed.) A more sophisticated model involves a structure where only one of the two Na atoms substitutes an Al atom, in the same way as in the $\sqrt{3}$ structure, whereas the second one in the unit cell is adsorbed on hollow sites of the underlying Na-Al layer. Such a model can in fact explain the STM topographs. In addition, it leaves enough freedom to adjust the Na-Na distance by varying the adsorption height of the second Na atom. This model is shown in Fig. 14 on the right-hand side, while on the left-hand side the $\sqrt{3}$ structure is shown for comparison. Na atoms are sketched as gray or black filled circles for substitutional or adsorbed Na atoms, respectively, first-layer substrate atoms as smaller open circles.

This structure has direct implications for the mechanism of the $\sqrt{3} \rightarrow (2\times 2)$ structural transformation. Since
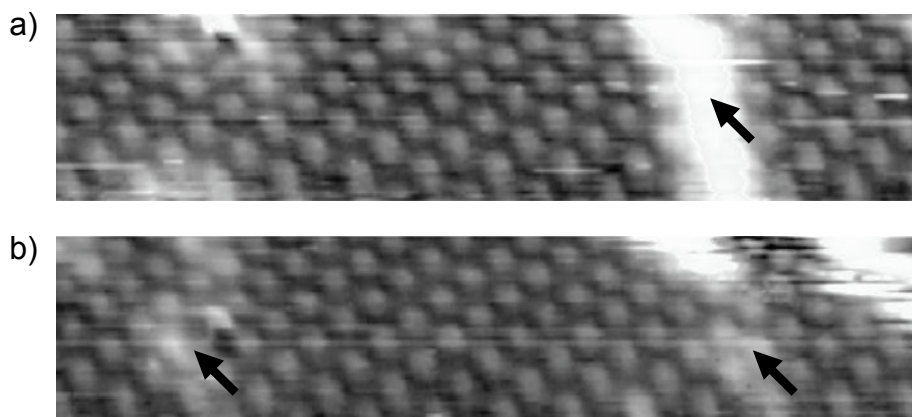
a)

b)

FIG. 13. Scanning-tunneling-microscopy images resolving the atomic structure of the (2×2) phase show one protrusion per unit cell, bright lines (marked by arrows) represent domain boundaries [(a) and (b) I_t=0.3 nA, V_t = -1.5 V, 116×25 Å].

the density of substitutional Na atoms is lower in the (2×2) structure additional aluminum atoms are needed for the transition from the $\sqrt{3}$ into the (2×2) phase, i.e., part of the Al vacancies have to be filled with Al atoms. From the densities of substrate atoms in the topmost layers of the two structures, $\frac{2}{3}$ ML and $\frac{3}{4}$ ML, respectively, $\frac{1}{12}$ ML Al atoms have to be filled in into the $\sqrt{3}$-covered surface in order to fully transform it into the (2×2) structure. These atoms can either originate from steps or be removed from the terraces, which would lead to holes on those terraces. Figure 15 shows that there are indeed holes created on a large terrace when the sodium coverage of the surface reaches 0.5 ML. These holes appear black in Fig. 15 and are imaged exactly one-monolayer deep, hence they are equally covered by the (2×2) structure, as is the terrace. Such holes are extremely rare on clean surfaces, and their high concentration is also different from that with the $\sqrt{3}$-covered surface. We, therefore, interpret them as the consequence of the need of substrate material in the transformation from the $\sqrt{3}$ into the (2×2) structure. The less darker areas (1.1 Å lower than the terrace level), which appear around some of the holes, are $\sqrt{3}$ patches which have not yet

transformed into the (2×2) phase. The bright areas, on the other hand, are $\sqrt{3}$ islands which are one atomic layer higher than the (2×2) terrace. The fractional coverages of the different phases in Fig. 15 are 73% for the (2×2) area of the large terrace, 7% for the $\sqrt{3}$ area on the terrace level, and 6% for the (2×2)-covered holes. This value for the area covered by holes agrees quantitatively with expectations for Al coverages of $\frac{2}{3}$ and $\frac{3}{4}$ ML in the topmost layer of the two phases, if we assume mass transport to be local, i.e., to be restricted to the (1000 Å)^2 terrace. The $\sqrt{3}$ islands, which most probably are relicts of the formation of the $\sqrt{3}$ phase from the clean surface, were assumed to be unchanged in size. The most important observations for deriving a model for the (2×2) structure are, therefore, a hexagonal rotational symmetry
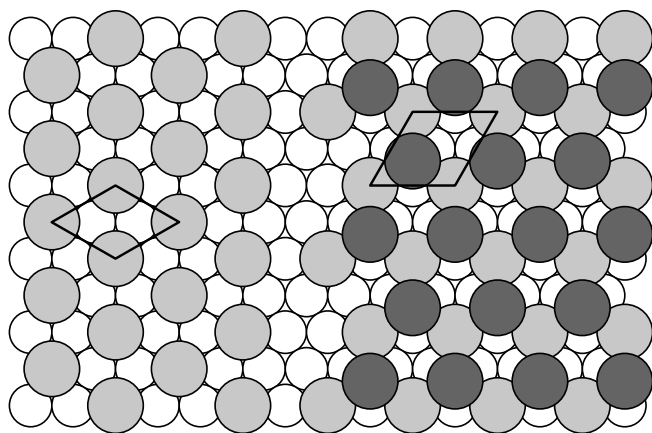
FIG. 14. Proposed model for the (2×2) structure with two Na atoms per unit cell: one Na atom is on a substitutional adsorption site (gray), the second one is adsorbed (black). For comparison, the $(\sqrt{3}\times\sqrt{3})R\,30°$ structure is shown on the left-hand side.

FIG. 15. Scanning-tunneling-microscopy image of the almost completely (2×2) Na-covered Al(111) surface, demonstrating the Al mass transport involved in the transformation from $\sqrt{3}$ structured into (2×2) structured. This leads to the creation of holes in the central areas of terraces [Θ=0.5, LEED sharp (2×2) spots, I_t=0.3 nA, V_t = -1.5 V, 980×1090 Å].

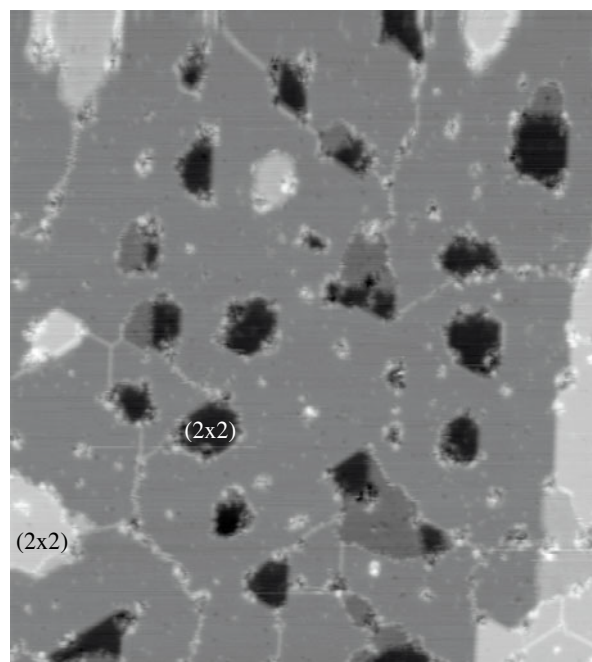of the topmost layer and the number of three Al atoms per unit cell contained in the adsorbate layer as deduced from the observed mass transport.

IV. DISCUSSION

A. The structure of the $(\sqrt{3} \times \sqrt{3})R\,30°$ phase

The peculiarities of the $\sqrt{3}$ phase formed by Na on Al(111) at $T = 300$ K have only recently been explained by introducing a reconstructed structure model where one Al atom per surface unit cell is replaced by a Na atom.[14,18,19] Reconstruction came as a surprise for alkali-metal adsorption on hexagonally close-packed surfaces, and it is even more surprising for the case of aluminum with its near-free-electron character, and also from the fact that bulk alloys between aluminum and sodium do not exist. The STM data presented here do, however, clearly support this model.

The most obvious evidence from the STM data for a substitutional adsorption site is the fact that the Na atoms are found to be in phase with the Al atoms of the topmost substrate layer. In principle, this lateral position would also be compatible with an on-top adsorption site. Such a position has actually been observed to be occupied by larger alkali atoms on hexagonally close-packed surfaces, e.g., for Cs on Cu(111),[11] and on Ru(0001).[12] For the system Cs/Ru(0001), it has been argued that the on-top site maximizes the screening of the dipole-dipole repulsion, due to a Ru atom situated between adjacent Cs atoms in the (2×2) structure, whereas for the geometrically favorable hollow position there are only hollow sites between two adsorbed alkali-metal atoms which cannot screen the dipoles as efficiently. On the other hand, for the $\sqrt{3}$ structure of Cs there is no difference in screening for the two sites and, consequently, the one with the higher coordination, i.e., the hollow site, is populated by the Cs atoms.[12] Similarly, screening is not improved by on-top adsorption in the Na/Al(111)-$\sqrt{3}$ structure, so that from screening arguments the on-top site is not plausible in this case. In accordance with these qualitative arguments, this site has been calculated to be the energetically most unfavorable one.[14,18] Experimentally, the on-top site has been excluded by the angular dependence of the SEXAFS signal.[14] In combination with these arguments, the lateral position identified by STM provides clear evidence for a substitutional adsorption site.

The assignment of a substitutional site is supported by the following experimental observations: (i) the presence of net attractive interactions between the Na atoms, as indicated by the formation of $\sqrt{3}$ islands from very low coverages on, (ii) the relatively low mobility of the Na atoms, and (iii) the mass transport of the Al atoms during formation of the $\sqrt{3}$ and (2×2) phases. This shall be discussed below. Furthermore, a significant activation barrier is expected for the Na atoms to substitute an Al surface atom, which had been predicted also from theory.[18] This could not be observed directly in our room-temperature experiments, but the preferential formation of the $\sqrt{3}$ islands at descending steps is strong indirect evidence for an activation barrier for the $\sqrt{3}$ formation.

The interactions between alkali-metal atoms adsorbed on (close-packed) metal surfaces are usually dominated by dipole-dipole repulsion. These repulsive interactions lead to 2D gas phases at low coverages and only with increasing coverage liquidlike structures with quasihexagonal geometry with ring-shaped LEED patterns are formed, in which the alkali-alkali distances for given coverages are maximized.[37,38] For Na on Al(111), however, there must be a net attractive interaction in order to rationalize the island formation seen in STM. It is clear, in a zero-order approximation, that in this case the dipole-dipole repulsion between the partly ionic Na adatoms, which, of course, is still present, is screened by embedding the adatoms into the surrounding Al atoms. But this does not explain the net attractive interaction for Na in the substitutional $\sqrt{3}$ geometry. A more detailed understanding comes from ab initio calculations by Neugebauer and Scheffler,[18,39] which showed that Al vacancies arranged in a $\sqrt{3}$ geometry are by 0.25 eV per vacancy site more favorable than in a (2×2) arrangement, hence there are net attractive interactions between vacancies in a $\sqrt{3}$ arrangement. From this energy balance, Neugebauer and Scheffler postulated that islands should be formed from the lowest coverages on.[39] The STM results confirm this prediction. For sodium adsorbed at on-top or on hollow positions, on the other hand, a net repulsion has been found in the calculations[18] in agreement with experimental findings in most alkali-metal adsorbate systems.[38]

Two other consequences of the substitutional reconstruction model that were mentioned above, a significant activation energy connected with its formation and a reduced mobility of the adsorbed Na atoms, shall be discussed later (in Secs. IV C and IV D). Both are confirmed by the STM data. Here, we will just mention that we hold the activation energy for the Na atoms to replace the Al surface atoms to be responsible for the preferential formation of the $\sqrt{3}$ structure at steps, and that the surface motion of Na follows a mechanism completely different from ordinary adsorbate diffusion.

Finally, the substitutional structure requires substantial mass transport of Al atoms: For a complete $\sqrt{3}$ layer one-third of the Al surface atoms have to be removed. However, because of their high mobility—a barrier for diffusion of Al atoms on Al(111) of only 0.04 eV has been calculated by Stumpf[40]—the Al atoms released during the reaction with Na can move to adjacent steps or will condense with other Al atoms and form Al adatom islands. These structural changes should be detectable by STM. We found, in fact, small Al plateaus on the $\sqrt{3}$ surface (see, e.g., Fig. 2) , which are usually not found on the clean surface and are, therefore, correlated with the formation of the $\sqrt{3}$ phase. However, the area covered by these Al plateaus is considerably smaller than expected from the change in Al surface density of $\frac{1}{3}$ ML. Hence, because of their very high mobility, most of the expelled Al atoms reach step sites where they are efficiently trapped. Since the deposition of the sodium could not be performed in situ in the STM, the resulting step motion could not be detected directly. This very much resembles the situation for the alkali induced

reconstruction of Cu(110), where mass transport could equally not be detected directly by the STM.[31] In the present case trapping at steps could even be more efficient due to preferential $\sqrt{3}$ nucleation at steps, so that most of the released Al atoms remain in the vicinity of steps (see Sec. IV D). Because of these effects the observation and quantitative evaluation of mass transport is not possible in the low coverage regime. However, both explanations for the reduced detectable mass transport are only valid as long as a sufficiently large part of the surface is still bare Al. When most of the surface becomes covered by the $\sqrt{3}$ phase the mobilities of the Al adatoms as well as of the substitutional Na atoms are drastically reduced as was demonstrated by the data in Sec. III E. This allows us to detect the mass transport connected with the $\sqrt{3} \rightarrow (2 \times 2)$ transformation on larger terraces.

The adsorption geometry for Na on the Al(111) surface is shown in Fig. 16 in a side and top view. The vertical distance to the first layer Al atoms of 1.7 Å is taken from the bond length derived from SEXAFS results.[14] (A recent LEED-IV study came to a lower value of 1.47 ± 0.02 Å.[19]) The Na atom is by 1.2 Å closer to the surface in the substitutional site as for the hollow site with the same bond length which enables effective dipole screening by the surrounding Al atoms. It should be noted that the substitutional site is not only more stable in a $\sqrt{3}$ geometry, but that, also, a single Na atom is assumed to be stabilized on this position with respect to adsorption on threefold and onefold hollow and on-top positions due to its much higher coordination.

In general, one could expect that for an increasing atomic radius the alkali-metal atom is more and more restricted to dive into the substrate vacancy, so that the energy gain by the effects described above no longer counterbalances the costs for vacancy creation and, hence, substitutional adsorption becomes less favorable. In contrast to this view, however, it turns out that also bigger alkali-metal atoms induce a reconstruction of the Al(111) surface at room temperature. Potassium atoms, e.g., reside at on-top positions only at low T (90 K); this metastable site converts into the substitutional one upon annealing to, or adsorption at, 300 K.[36] This change is seen also in high-resolution core-level spectra by going from 100 to 300 K.[22] From core-level spectra for Rb and Cs it has been concluded that these also induce a recon-

struction of the Al(111) substrate at 300 K.[22] For Rb this has been confirmed in a recent LEED-IV analysis, which showed that Rb atoms occupy quasisubstitutional sites in the $\sqrt{3}$ structure on Al(111) at 300 K.[41] A recent NISXW study also finds substitution for Rb/Al(111) at 300 K.[42] (This study corrects the former interpretation of on-top adsorption being stable up to 300 K.[13]) Thus from an experimental point of view, Na, K, and Rb populate the on-top position at low T, which is metastable and converts to a site above a vacancy in the Al(111) substrate for room temperature. The existence of metastable sites reflects the activation energy required for the reconstruction.

Density-functional theory calculations show, in agreement with experiment, that the substitutional site has lowest energy for Na.[18] For potassium, on the other hand, the hollow, on-top and substitutional site were found to be practically degenerate by Neugebauer and Scheffler. Thus the phase transition of a K adlayer to reconstruction has been considered to be a collective effect of the periodic layer.[36] For Na, the STM results demonstrate that even an isolated Na atom rests on its substitutional site when traveling together with the underlying vacancy between adjacent islands (see also Sec. IV C).

In conclusion, the substitutional model for the $\sqrt{3}$ phase, which was first derived from SEXAFS,[14] is confirmed by the STM measurements.

B. Imaging of Na in the $(\sqrt{3} \times \sqrt{3})R 30°$ structure by STM

The imaging of adsorbed alkali metals by STM is a complex problem. From their electronic structure—in theoretical studies they are generally characterized by strong s resonances directly above the Fermi level—it was predicted that distinct protrusions at the location of the alkali atom should be seen in the STM contours.[43,44] Similar electronic properties were also found for Na on Al(111): it was found by IPS (inverse photon electron spectroscopy) that Na adsorption on Al(111) leads to a significant increase of state density at 1 eV above E_F,[45] in accordance with the calculations by Lang and Ishida.[46,47] If this increase in the LDOS contributes to the tunnel current, it could cause the observed imaging of sodium as protruding areas. On the other hand, in the systems that have been studied experimentally [Cu(110) (Ref. 31) and the three low-index surfaces of Au (Ref. 32)] the alkali-metal atoms mostly did not contribute to the contours of constant tunnel current. Though in part of the cases, e.g., for Au(111) with $\Theta_{alkali} < 0.2$ or for Au(110) with $\Theta_K < 0.25$ this apparent "transparency" is more a nonresolution of the alkali-metal atoms due to their high mobility which prevents their detection on these surfaces. There are other experimental cases where the alkali-metal atoms appear transparent in spite of the fact that they are highly localized due to their embedding into the troughs of the (alkali-induced) reconstructions. In these missing-row reconstructions the position of the alkali atom is relatively deep inside the surface as compared to the position on a jellium surface. In addition, it has recently been
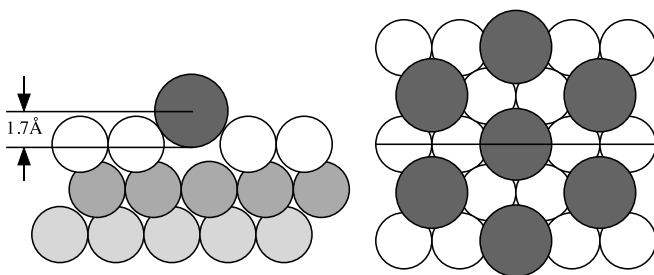

FIG. 16. Structural model showing the adsorption geometry for Na atoms substituting Al atoms on the Al(111) surface, see Ref. 14. Open and light gray circles represent Al atoms in the first and subsequent layers, respectively; larger gray circles correspond to Na atoms.

suggested[33] that adsorption in this position (namely, that of a K atom inside the missing-row troughs of the reconstructed Cu(110) and Au(110) surfaces) significantly affects the electronic structure of the alkali-metal atom: Because of the higher coordination of the alkali-metal atom and, hence, of a stronger chemical bond to the substrate, the s resonance is shifted away from E_F. It contributes, therefore, much less to the tunnel current as compared to an alkali-metal atom on a nonreconstructed surface, with the result of the alkali-metal atom becoming "transparent" to the STM.

Interestingly, the imaging of the Na atoms on the substitutional sites on Al(111) follows at least qualitatively the prediction by Lang.[43] We find that for gap resistances of 1×10^8 Ω to 1×10^{10} Ω the Na atoms are represented by protrusions in the STM contours. Although the absolute height for large tip-to-sample distances was found to depend on the tip conditions, the fact of a positive variation in the STM contours was reproducible. We, therefore, rule out effects of contaminations of the apex of the tip which would have led to qualitative changes in the imaging conditions when the state of the tip changed. Quantitative comparison with Lang's calculation is problematic since they did not include reconstruction, i.e., the Na atoms were adsorbed on a jellium surface and not embedded into it. Nevertheless, the qualitative agreement is remarkable since, in the present case, the alkali-metal atom sits on a site deep in the substrate, similar to the missing-row reconstructed Cu and Au surfaces, and it might be expected that similar effects are present in these two cases. At present, we can only speculate about reasons for the differences in the imaging conditions between Na on Al(111) on the one hand and various alkali metals on Cu(110) and Au(110) on the other. The bond strength of the Na atoms to the Al atoms surrounding the vacancies is probably comparable to that of the alkali metals in the missing-row troughs of Cu and Au. One difference is, however, that despite the substitutional site the Na atom is located much further above the surface (1.7 Å) as compared to the K atoms on Cu(110) (1.1 Å).[48] A further difference is of course the absence of d electrons in the case of Al. If d states contribute significantly to the bonding of the adsorbed alkali metal to the surface, this would also contribute to the differences observed experimentally.

The imaging of the Na atoms in the experiments becomes more complex by the observation that the apparent height of the Na atoms varies with the tunneling conditions. With decreasing gap resistance (from 2×10^{10} Ω to 2×10^7 Ω) the apparent height difference between Na and the substrate continuously decreases from more than 3 Å to less than the geometric height, e.g., to 0.5 Å in Figs. 3 and 6 and even to -0.1 Å in Fig. 5. Most simply one would attribute these effects to a locally reduced barrier height above the sodium-covered areas reflecting the work function decrease by Na adsorption. However, the relation of the local barrier height measured in the STM experiment to the (macroscopic) work function is not trivial.[43] [See, e.g., the measured local barrier height of 1–3 eV for the clean Al(111) surface[28] versus its work function of $\Phi_{Al} = (4.23 \pm 0.03)$ eV.[49]] Ab-

solute values for the work function can, therefore, not be derived from measurements of the local tunneling barrier. Nevertheless, the observed variation of imaging height with distance leads to a ratio of local barrier heights for adsorbate covered to clean substrate areas of 0.6 ± 0.1 (assuming local barrier heights of 1–4 eV for the substrate). This agrees well with the ratio of the macroscopic quantities of $\Phi_{Na}/\Phi_{Al} = 0.63$ [Na adsorption reduces the work function by 1.6 eV (Ref. 24)]. Bearing in mind that the picture of local barrier heights contains the simplification of neglecting tip-sample interactions, which become important for close tip-sample distances, it explains the observed imaging quite well for the wide range of gap widths investigated. It is interesting to note that the inverted imaging corresponds precisely to the distribution of the charge density calculated by Neugebauer and Scheffler for the present system,[18] but again care has to be taken since due to tip-sample interactions at small gap widths the tip no longer probes the unperturbed local state density of the sample surface.

In total, imaging of Na in substitutional positions arranged in the $\sqrt{3}$ structure on the Al(111) surface by STM is characterized by a Na induced increase in the tunnel current leading to protrusions in the STM image, and by a continuous decrease of the apparent height of the Na atoms from 1.3 to -1.7 Å relative to their actual position with decreasing gap width. The latter effect can partly be understood from the locally reduced barrier height for the tip above Na-covered surface areas, due to the work function decrease by alkali-metal adsorption. The imaging behavior found here is different from that for alkali metals on the fcc(110) surfaces of Au and Cu, where the alkali-metal atoms are similarly embedded into the reconstruction troughs of the substrate.

C. Mobility of the substituting Na atoms

The question of the mobility of the Na atoms at coverages below 0.33 is crucial for the understanding of the $\sqrt{3}$ formation mechanism and shall, therefore, be discussed first. From the observation of bright stripes in the scan lines and from the exchange of Na atoms between the $\sqrt{3}$ islands, a diffusion constant (at 300 K) of 6×10^{-15} cm^2/s $\leq D \leq 2 \times 10^{-13}$ cm^2/s has been derived above. In contrast, a diffusion barrier of below 0.03 eV has been calculated for Na adsorbed on the nonreconstructed Al(111) surface.[35] With a standard value for the attempt frequency ($\nu_0 = 1 \times 10^{12}$ s^{-1}) this corresponds to a diffusion constant of about 5×10^{-5} cm^2/s at 300 K, i.e., the diffusion constant of "free" Na atoms is by eight to ten orders of magnitude larger than the numbers obtained here. This agrees with experimental findings for other alkali-metal adsorption systems, where similar values were obtained, for instance, for K on Ru(0001) with diffusion constants between 10^{-7} and 10^{-5} cm^{2}s^{-1} at 300 K.[50] (The actual number was found to depend on the K coverage.) Hence the diffusing species for $\Theta_{Na} < 0.33$ on Al(111) must be distinctively different from the highly mobile alkali adatoms in other systems. This suggests that the diffusing species is not the Na atom alone but that the complete adsorption complex is moving, i.e., the Na atom together with the underlying Al va-

cancy in which it is adsorbed. This interpretation is supported by the observation of comparable imaging heights for the mobile Na species and for Na in the $\sqrt{3}$ islands, indicating that the mobile Na species resides on the same substitutional sites as the atoms in the $\sqrt{3}$ islands. This is a remarkable result, it means that even a single Na atom is able to locally create or maintain a reconstruction of the close-packed Al surface, similar to previous observations for K/Cu(110).[31]

Of course we cannot exclude that a small amount of Na present on the surface, which is not detectable, e.g., by comparison of AES and STM derived coverages, always exists in the highly mobile adsorbate state *on* the nonreconstructed surface. In fact, directly after deposition, the Na must actually be in such a state, in which it very efficiently "searches" energetically favorable sites where it can be incorporated into the first Al layer. These processes are, however, terminated at the time when the STM experiments were started, typically several minutes after the deposition. In spite of its lower mobility, motion of the substitutional Na plays an important role for the growth of the $\sqrt{3}$ islands (see below). The mobility of the substitutional Na is further reduced once they are incorporated into $\sqrt{3}$ islands. The stability of the atomic features inside the $\sqrt{3}$ islands, as seen in the STM images demonstrates that those Na-vacancy complexes which are completely surrounded by the same species are immobile. They are only mobile when they are on free surface areas or at the edges of islands, i.e., to be mobile they have to be completely or partly surrounded by areas of the nonreconstructed Al surface.

Finally, we want to comment on the mechanism of the diffusion process. In principle, diffusion of a Na-vacancy complex includes the creation of a new vacancy, jumping of the Na atom into that vacancy site and filling of the old vacancy by a neighboring Al atom. Different mechanisms are conceivable for such a process. The first one follows exactly the above sequence, i.e., a vacancy is created first, by removing an Al surface atom, the Na atom moves over into the vacancy and the remaining Al vacancy is filled up by another Al atom. Energetically most costly in this sequence is the formation of a vacancy, i.e., the creation of a "surface Frenkel pair." For Al(111) this had been calculated to cost about 1.2 eV.[18] In a second possible way, which is a two-step process, the vacancy is first filled by a neighboring Al atom and, at the same time, the Na atom is lifted from its position inside the vacancy to a position above the surface. In a second step, the Na atom jumps into the vacancy at the new position. The activation energy for such a process can be estimated from the sum of the diffusion barrier for the vacancy and of the difference of the adsorption energies of a Na atom inside the vacancy and on a surface position. Also these quantities have been calculated recently: For a diffusion barrier of a vacancy in the Al(111) surface a value of 0.56 eV (Ref. 40) was obtained, and for the difference in adsorption energies of the Na, in the vacancy and on the surface, numbers between 0.57 and 0.71 eV were calculated.[18] (The actual value depends on the position to which the Na atom moves on the surface, i.e., to a hollow or an on-top site.) As a result, the activation energy for this process should certainly be larger than 1 eV as well. These numbers can be compared to the diffusion barrier for the Na-vacancy complex which is estimated from the STM data. Assuming an attempt frequency for single atom jumps of $\nu_0 = 1 \times 10^{12}$ s^{-1}, we obtain a value of $E_m = (0.55 \pm 0.05)$ eV from the diffusion constant derived from STM observations. Hence the experimentally determined activation barrier is considerably lower than that estimated from the theoretical numbers for plausible multiple-step processes. This suggests that the movement of the vacancy and the Na occurs by a concerted mechanism through an exchange process (see Fig. 17), which is expected to be associated with a lower barrier.

A diffusion mechanism consisting of the concerted exchange of adsorbate and substrate, as it is proposed here, has been observed by FIM (field-ion microscopy) for Pt atoms on a Ni(110) surface.[51] This finding has been proposed to account for the surprisingly low migration barrier perpendicular to the close-packed [1$\bar{1}$0] rows of fcc(110) surfaces comparable to the one along these rows, as observed, e.g., for W/Ir(110).[52] In fact, recent theoretical results suggest that diffusion via an exchange mechanism is quite common for metal on metal diffusion.[53] In our case, the concerted motion of the adsorbed Na atom together with the underlying Al vacancy similarly provides the advantage of an increased coordination in the transition state which is the reason for the reduced activation energy compared to a two-step process. Furthermore, so far, lower preexponentials have been found for exchange diffusion[53,54] and it is reasonable to assume this also for the present case. This leads to a reduction of the value for the migration barrier derived from our value of the diffusion constant. For instance, using a value of $\nu_0 = 7 \times 10^5$ s^{-1} (Ref. 54) yields an activation energy of $E_m = (0.25 \pm 0.05)$ eV for Na/Al(111) at 300 K.

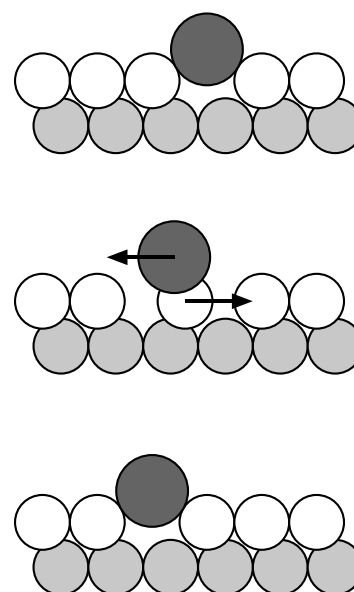In conclusion, the diffusion of Na on the Al(111) sur-

FIG. 17. Schematic representation of the concerted motion of Na (dark) and the underlying Al vacancy during diffusion of substitutional Na atoms, which is expected to be associated with a lower barrier than a two-step process.

face follows a mechanism which consists of the motion of Na/Al-vacancy complexes. We find that the rather low diffusion barrier of this species can only be explained by assuming a concerted motion of the Na atom and one of the neighboring Al surface atoms. Stabilization by attractive interactions reduces the mobility in the $\sqrt{3}$ phase and at the perimeter of the $\sqrt{3}$ islands. This mechanism is effective only as long as the complete surface is not covered by the $\sqrt{3}$ phase. At this point, the mobility of all surfaces species is significantly reduced.

D. Nucleation and growth of the $(\sqrt{3} \times \sqrt{3})R\,30°$ phase

The basic process for the formation of a unit of the $\sqrt{3}$ structure is the substitution of an Al atom in the first layer by a Na atom. A rough estimate of the activation energy for such a process can be made be separating it into several consecutive steps. A natural guess would be that, at first, an Al atom is removed from its site *in* the topmost layer on a terrace to a position *on* that layer. In a second step, a Na atom jumps from a position on the nonreconstructed terrace into the vacancy, and third, the Al atom released moves to a step edge to which it becomes attached. It is then clear that the largest activation energy is connected with the first step, i.e., the creation of a surface Frenkel pair, which requires an activation energy of 1.2 eV.[18] The energies of the two other steps are negligible if compared with this value. This barrier is too high to be easily overcome at room temperature. A lower barrier will result if (i) the exchange process occurs in a concerted motion, with the Na atom directly replacing the Al surface atom, or (ii) if the exchange process occurs at defects such as step edges, which had been suggested before for this process.[18] A third possible way of creating substitutional Na is the attachment of adsorbed Na to the ascending step together with mobile Na atoms, which either stem from process (i) or diffuse along the steps, as also occurs on the clean surface.

The first possibility for reducing the barrier height for an exchange on a flat terrace appears very plausible since in this case part of the incorporation energy of the Na surface atom is released already in the transition state, thus lowering its energy. In fact, a similar mechanism had been suggested for the K-induced reconstruction of Cu(110), where at low coverages individual K atoms create a local reconstruction nucleus by exchanging with Cu surface atoms.[31] A second example for such a mechanism is well known from surface diffusion of metals, where diffusion by exchange had been found experimentally, e.g., by FIM experiments,[51,52] and in theoretical studies.[53] Hence a significant reduction of the barrier height as compared to the barrier for the creation of a surface Frenkel pair is expected also in the present case. It will be shown below that this process does indeed contribute to the growth of the $\sqrt{3}$ islands. This means that highly mobile Na adatoms, which diffuse over the terraces, have a certain chance to undergo an exchange reaction. The substitutional Na atoms formed after this reaction are still sufficiently mobile to continue migrating over the surface, until they reach the edge of a $\sqrt{3}$ island

and get incorporated, due to the attractive interactions responsible for island growth, or until they meet another Na_{subst} and coalesce into a small nucleus, which can grow subsequently by incorporation of additional Na_{subst}. The Al atoms released in the exchange processes are also highly mobile on the surface[40] and can at least, at not to high $\sqrt{3}$ coverages, reach the nearest step where they get incorporated.

In the second mechanism suggested above exchange occurs at defects, preferentially at steps, exploiting the lower coordination of Al atoms there. Again it is plausible that the barrier for exchange will be significantly lower compared to the value of 1.2 eV for the creation of a surface Frenkel pair. From plausibility arguments, but also from comparison with exchange processes at step edges in metal diffusion,[55] we expect a slightly different reaction pathway in this case. Rather than being expelled onto the upper terrace, the Al step atom presumably is moved outward onto the lower terrace when the Na sinks into the surface layer. The Na_{subst} complexes then either cluster directly at the step, on the upper terrace side, or they move away from the step forming Na_{subst} species on the terrace.

Despite of the observation that the $\sqrt{3}$ islands nucleate preferentially at steps, most of them are attached to steps, our results do not allow to decide which of the two mechanisms for exchange dominantly takes place. Also for homogeneous exchange reactions on the terraces nucleation of $\sqrt{3}$ islands may preferentially occur on the upper terrace side of steps. Further growth of the $\sqrt{3}$ islands proceeds by incorporation of additional mobile Na_{subst}, which had been created at step edges or homogeneously on terraces, or by exchange reactions at the island perimeter. It can occur also in the way that Na_{subst}, which had been formed at steps near the intersection of a $\sqrt{3}$ island with the step, do not migrate out into the bare terrace but along the island edge.

Once the $\sqrt{3}$ islands are formed they tend to maintain rather compact shapes. The Na_{subst} are sufficiently mobile also along the island edges for this to occur, as seen in the STM images as fluctuations of the island edges. The driving force for this tendency to minimize the island perimeter for a given area results from the attractive interactions between the Na_{subst} species in the $\sqrt{3}$ islands. This favors high coordination numbers and, therefore, compact islands. Both the mobility of the Na_{subst} and the tendency of forming compact $\sqrt{3}$ islands prevent this phase from growing in narrow stripes along steps, which would block these steps for further exchange processes.

The mechanism for the $\sqrt{3}$ formation resembles the picture of the standard 2D nucleation and growth theories, as they are applied, e.g., for the description of epitaxial growth, with the difference that the mobile species in this case are not adatoms but substitutional atoms and the nucleating species—Na_{subst}—may not be created homogeneously all over the surface, but may preferentially form at steps. Based on these ideas, we can also understand the relatively low density of $\sqrt{3}$ islands and the experimental observation that Na free areas exist at the steps up to coverages close to completion of the

$\sqrt{3}$ layer, e.g., in Fig. 2. Nucleation is only possible in the early stages of deposition, when the density of islands is still too low that the island edges can be reached by the diffusing Na_{subst} species. This can be understood in terms of a depletion zone surrounding each stable nucleus, where the density of mobile species is reduced and, therefore, nucleation of a new island is very improbable. The rather large distance between the $\sqrt{3}$ islands in our case is a direct measure for the rather high mobility of the Na_{subst}.

Based on these ideas, we also want to comment on the experimental observation that the terrace area along the ascending steps is free of $\sqrt{3}$ phase up to rather high coverages. Depletion zones along ascending steps are commonly found in epitaxial growth where these steps act as sinks for diffusing adatoms, and one may speculate whether, also, in this case, ascending steps act as trap for diffusing Na adatoms, where these are incorporated into the upper terrace layer, together with mobile Al adatoms. This way, also, the density of Na_{subst} would be reduced in an area along ascending steps, making nucleation of $\sqrt{3}$ islands in this area improbable.

In summary, Na exchange can occur either homogeneously in the flat terraces, in a correlated motion of the atoms involved, or at defects such as steps. The resulting Na_{subst} are mobile and nucleate islands of the $\sqrt{3}$ phase, preferentially at descending steps. These islands grow by incorporation of additional mobile Na_{subst} species. The low density and the compact shapes of the $\sqrt{3}$ islands can be explained by the mobility of Na_{subst} species on the flat terraces or along island edges, respectively. This mobility was observed also directly as fluctuations of the $\sqrt{3}$ islands sizes and shapes.

E. The (2×2) structure model

The STM images show that the (2×2) phase has a hexagonal symmetry and is characterized by one protrusion per (2×2) unit cell. Islands of the (2×2) phase appear by about 1.2 Å higher in the topographs than the surrounding $\sqrt{3}$ phase. During its formation from the $\sqrt{3}$ structure, it is observed that holes are formed on large terraces. From the area of these holes, it was concluded that the $\sqrt{3} \rightarrow (2 \times 2)$ phase transition is connected with an increase of the density of Al atoms in the topmost substrate layer by $\frac{1}{12}$ of a monolayer. This amount corresponds to the transformation of a structure with a coverage of vacancies of $\frac{1}{3}$ into one with $\Theta_{vacancy} = \frac{1}{4}$. Based on these observations, the double-layer model shown on the right-hand side in Fig. 14 is proposed. In this model, one Na atom per unit cell is on a substitutional position, similar to that in the $\sqrt{3}$ structure, the second one is on a surface site above that layer. The nearest-neighbor distance between sodium atoms is then determined solely by the vertical position of the Na atoms. If it is assumed that the Na atoms are represented equally in the $\sqrt{3}$ and the (2×2) structure by the STM (i.e., equal electronic effects, etc.) so that the STM contour would in fact reflect the relative adsorption heights, the apparent height difference of 1.2 Å would correspond to an Na-Na distance of 3.5 Å, which appears reasonable considering the

Na bulk value of 3.66 Å.

In former studies, several models have been proposed for the (2×2) phase. From its coverage of 0.5, Porteus had suggested that the (2×2) LEED pattern might be a superposition of the LEED patterns of three domains of a (2×1) structure,[23] which was later concluded also by a second group.[56,57] Such an explanation can, however, be ruled out from the present STM data. The periodicity of the phase and its symmetry, which does not change with the tunneling conditions, is clearly that of a (2×2) structure.

Hohlfeld and Horn were the first to introduce a bilayer model for the (2×2) phase.[24] It consists of two layers of Na on top of each other, with $\Theta = 0.25$ each, adsorbed on a nonreconstructed substrate. This could account for our finding that there is only one protrusion per unit cell in the STM topographs. However, from the mass transport seen by STM, which led us to conclude that the (2×2) phase must contain Al vacancies though at a different density than in the $\sqrt{3}$ phase, the (2×2) structure must be reconstructed.

The most recent proposal for a (2×2) structure model came from an investigation using standing x-ray wavefield absorption.[20] The model consists of two mixed layers of Na and Al atoms on top of each other, both with a stoichiometry of Na_1Al_2. The registry is such that the Na atoms of each layer sit directly above Al atoms of the underlying layer, whereas the Al atoms are located on hollow sites. This model accounts for the intermixing as deduced by XPS,[21] and it is in agreement with the hexagonal symmetry of the structure as seen in the STM topographs. However, there are also some observations which cannot be reconciled with this model: First, the model has a density of Al atoms of 1.0 if the two reconstructed layers are counted together. This is in contradiction to the finding by STM that $\frac{1}{4}$ of the surface Al atoms are missing in the (2×2) phase. Second, as we found by LEED (Sec. III A), the (2×2) structure is less stable against annealing than the $\sqrt{3}$ structure, and TPD data show that there are two desorption peaks of Na from the (2×2) phase.[29] This is compatible with a (2×2) structure involving two different Na species one of which is considerably less firmly bound than the other one, although, in principle, a two peak spectrum can be explained also on the basis of strongly repulsive interactions, which act only in the higher coverage structure.

By our model we can explain the fact that the Na $2p$ core-level spectra reported by Andersen et al.[21,22] showed two distinctly different binding states of Na to the Al surface for adsorption at 300 K. One was characterized by a peak at 31.1 eV, and was present from low coverages on, while a second at 30.6 eV appeared in the spectrum for $\Theta_{Na} = 0.38$. It was found that the higher-energy peak disappears when the (2×2) structure is covered by Cs.[22] Therefore this peak was assigned to Na in the surface layer, whereas the peak with lower energy was attributed to Na in the lower layer of the bilayer structure. In accordance to the two-peak spectra, our structure model contains two Na species with different coordination to Al. In the model proposed by Kerkar et al.,[20] in principle, also two Na species exist. Na atoms in the first reconstructed

layer have eight Al neighbors (completely surrounded by Al) and those in the topmost layer have seven Al neighbors. This, however, appears to be only a minor difference, which would not be expected to lead to the observed pronounced difference in the Na 2p energies.

From the Al 2p core-level spectra reported by Andersen et al., strong intermixing was inferred for the (2×2) structure.[21] Two Al 2p peaks had been observed which had large shifts relative to the value of the clean surface ($\Delta E_1 = -0.17$ eV, $\Delta E_2 = -0.43$ eV). As a Na layer adsorbed on the unreconstructed Al(111) surface gave shifts of only 70–80 meV, this suggests that there are two Al species in the intermixed layer which differ very much in their coordination to Na. This cannot be reconciled with our model. The model by Kerkar et al.,[20] on the other hand, includes two Al species which are very similar in their coordination with respect to the Na atoms, which therefore also bears the problem of explaining two distinctly different Al 2p shifts.

The model proposed here for the (2×2) structure consists of a layer of Na atoms (0.25 ML) on substitutional sites as in the preceding $\sqrt{3}$ structure, and a second Na layer adsorbed on the hollow sites of the first. It is the most simple model which correctly describes the mass transport during the transition from the $\sqrt{3}$ into the (2×2) structure. It is also quite reasonable that most of the once substitutional Na atoms remain in this preferred position. That also the (2×2) structure contains Na atoms on substitutional sites is strongly supported by the observation of an unchanged Na-Al bond length and angular dependence of the SEXAFS signal for the (2×2) structure.[58] Note that in our model, also, the second-layer Na atoms have a bond length of 3.33 Å, so that there exists only one Na-Al bond length for both, Na in the first and second layer, respectively.

During submission of this paper a combined LEED-IV analysis, total-energy calculation,[26] and SEXAFS investigation[25] appeared which finds a bilayer model that differs from the model proposed in Fig. 14 in that the topmost layer contains, in addition to the Na atom, one Al atom per (2×2) unit cell. This model has also been found with x-ray photoelectron diffraction.[59] It is evident that this model is in better agreement with the Al 2p core-level shifts. The larger shift is due to Al atoms embedded in the surface layer, which are almost completely surrounded by Na. The smaller shift of 170 meV is attributed to Al atoms in the second layer to which the substitutional Na atoms are bound. This model is in agreement with the STM imaging of one protrusion per unit cell. Recent density-functional calculations on the (2×2) structure show that most of the charge density is located at the surface Al atom[26] from which it could be concluded that the STM sees mostly the Al atoms. However, the mass transport detected from our STM data is considerably lower than the surplus of Al that is required by this model for the $\sqrt{3} \rightarrow$ (2×2) phase transition. Our estimate of the Al coverage in the (2×2) structure was based on the assumption that the mass transport remains local on a (1000 Å)^2 scale, which appeared plausible from the stability of the $\sqrt{3}$ reconstruction. In order to reconcile our data with the new (2×2) model, we have to assume

long-range mass transport and the involvement of atomic steps. One might therefore speculate that the mass transport which fills the vacancies is local, whereas mass transport in the much more dilute surface layer is of long range.

V. CONCLUSIONS

Na adsorption on Al(111) at 300 K was investigated by STM, both of the resulting two-ordered phases ($\sqrt{3} \times \sqrt{3} R 30°$ and 2×2) were found to involve a reconstruction of the substrate. Chemisorption proceeds via initial Na adsorption on top of the surface and subsequent rapid incorporation into that layer, leading to Na on substitutional sites, i.e., Na adsorbed in Al vacancies. Individual Na/vacancy complexes have attractive interactions and are mobile, which leads to island formation already for lowest coverages (e.g., 0.07 ML). Inside these islands the Na/vacancy complexes are immobile which allows to image their atomic structure. The lateral adsorption site has been determined as in phase with the Al lattice. From the terrace structure of the almost $\sqrt{3}$-covered surface there are indications of a larger scale rearrangement of the aluminum substrate. Together, these results confirm the idea of substitutional adsorption, i.e., the replacement of Al atoms by adsorbed sodium, as first proposed on the basis of SEXAFS data and total-energy calculations.

Due to the equal imaging height of the mobile Na species with the one localized in the $\sqrt{3}$ islands, it has been concluded that, also, the mobile species consists of a Na atom adsorbed above a substrate vacancy. This, however, means that a single Na atom maintains the reconstruction of the underlying substrate, even if it is isolated on a terrace. From this, the mechanism for the diffusion of Na on the Al(111) surface has been derived. It consists of the concerted exchange between the Na atom and one of the neighboring Al atoms. Observation of Na exchange between neighboring islands as well as direct evidence for these mobile species as stripes of increased height in STM images enable estimates for the diffusion constant for Na/Al(111) at room temperature to 6×10^{-15} cm^2/s $\leq D \leq 2 \times 10^{-13}$ cm^2/s.

The reaction of Al(111) with Na up to 0.33 ML proceeds via the following scenario, as derived from the STM data. Na first adsorbs on the unreconstructed Al(111) surface as a highly mobile species. These adatoms can exchange with Al surface atoms, either in a correlated process on the flat terraces or at descending steps. They can also assemble with mobile Al atoms at ascending steps. The resulting substitutional Na atoms, adsorbed on top of an Al vacancy, are sufficiently mobile to migrate over the surface. They can nucleate $\sqrt{3}$ islands, which occurs preferentially via heterogeneous nucleation at descending steps, or get incorporated into existing $\sqrt{3}$ islands when they reach an island edge. Following arguments of 2D nucleation and growth, the low density and the compact shapes of the $\sqrt{3}$ islands result from the mobility of the substitutional Na in the flat terraces or along the island edges, respectively. Due to the extended depletion zones around existing $\sqrt{3}$ islands (at descending steps) homogeneous nucleation on terraces is

possible only for larger terraces.

Upon reaching the ideal coverage of 0.33 ML for the $\sqrt{3}$ phase the Na-Al layer becomes more stable, diffusion processes are limited to exchange between neighboring $\sqrt{3}$ domains. Two types of domain walls are found, "light" and "heavy" walls, which differ by their local Na concentration. With increasing Na coverage, the latter ones become more frequent and are imaged increasingly high, up to the apparent height of the (2×2) phase. These "heavy" domain walls act as nuclei for the higher coverage (2×2) phase.

The phase transition from the $\sqrt{3}$ to the (2×2) structure involves substrate mass transport which is evident from the formation of one monolayer deep holes on large terraces. The amount of Al needed in this transition has been deduced to $\frac{1}{12}$ ML, which implies that the (2×2) structure contains three Al atoms per unit cell in the adsorbate-substrate layer. The STM images showed only one protrusion per (2×2) unit cell, and a sixfold rotational symmetry of the surface corrugation pattern. From these observations, a bilayer structure model for

the (2×2) unit cell is proposed consisting of a mixed Na-Al layer with Na atoms on substitutional sites as in the preceding $\sqrt{3}$ structure and a Na adlayer with Na atoms residing on top on the hollow sites of the first layer. This way, most of the substitutional Na atoms from the $\sqrt{3}$ phase can remain in this preferred position during the $\sqrt{3} \rightarrow (2 \times 2)$ transformation. This model is in accordance with the XPS data in the literature. It implies only one Na-Al bond length of 3.3 Å, in agreement with recent SEXAFS results. It disagrees, however, with a similar model proposed very recently, where the uppermost layer contains, in addition to one Na atom, one Al atom per unit cell.

ACKNOWLEDGMENTS

*Present address: Institut de Physique Expérimentale, Ecole Polytechnique Fédérale de Lausanne, PHB-Ecublens, CH-1015 Lausanne, Switzerland.

†Permanent address: Abteilung für Oberflächenchemie und Katalyse, Universität Ulm, D-89069 Ulm, Germany.

[1]J. W. Döbereiner, Zur Chemie des Platins in Wissenschaftlicher und Technischer Beziehung (Balz'sche Buchhandlung, Stuttgart, 1936).

[2]J. B. Taylor and I. Langmuir, Phys. Rev. 44, 423 (1933).

[3]R. W. Gurney, Phys. Rev. 47, 479 (1935).

[4]Physics and Chemistry of Alkali Metal Adsorption, edited by H. P. Bonzel, A. M. Bradshaw, and G. Ertl, Materials Science Monographs Vol. 57 (Elsevier, Amsterdam, 1989).

[5]H. Ishida, Phys. Rev. B 42, 10 899 (1990).

[6]E. Wimmer, A. J. Freeman, J. R. Hiskes, and A. M. Karo, Phys. Rev. B 28, 3074 (1983).

[7]D. M. Riffe, G. K. Wertheim, and P. H. Citrin, Phys. Rev. Lett. 64, 571 (1990).

[8]S. Modesti, C. T. Chen, Y. Ma, G. Meigs, P. Rudolf, and F. Sette, Phys. Rev. B 42, 5381 (1990).

[9]M. Scheffler, C. Droste, A. Fleszar, F. Máca, G. Wachutka, and G. Barzel, Physica B 172, 143 (1991).

[10]J. Bormet, J. Neugebauer, and M. Scheffler, Phys. Rev. B 49, 17 242 (1994).

[11]S. A. Lindgren, L. Walldén, J. Rundgren, P. Westrin, and J. Neve, Phys. Rev. B 28, 6707 (1983).

[12]H. Over, H. Bludau, M. Skottke-Klein, G. Ertl, W. Moritz, and C. T. Campbell, Phys. Rev. B 45, 8638 (1992).

[13]M. Kerkar, D. Fisher, D. P. Woodruff, R. G. Jones, R. D. Diehl, and B. Cowie, Phys. Rev. Lett. 68, 3204 (1992).

[14]A. Schmalz, S. Aminpirooz, L. Becker, J. Haase, J. Neugebauer, M. Scheffler, D. R. Batchelor, D. L. Adams, and E. Bøgh, Phys. Rev. Lett. 67, 2163 (1991).

[15]R. J. Behm, in Physics and Chemistry of Alkali Metal Adsorption (Ref. 4), p. 111.

[16]W. B. Pearson, Handbook of Lattice Spacings and Structures of Metals and Alloys (Pergamon, New York, 1967).

[17]J. V. Barth, H. Brune, R. Schuster, R. J. Behm, and G. Ertl, Surf. Sci. 292, L769 (1993).

[18]J. Neugebauer and M. Scheffler, Phys. Rev. B 46, 16 067 (1992).

[19]J. Burchhard, M. M. Nielsen, D. L. Adams, E. Lundgren, and J. N. Andersen, Phys. Rev. B 50, 4718 (1994).

[20]M. Kerkar, D. Fisher, D. P. Woodruff, R. G. Jones, R. D. Diehl, and B. Cowie, Surf. Sci. 278, 246 (1992).

[21]J. N. Andersen, M. Qvarford, R. Nyholm, J. F. v. Acker, and E. Lundgren, Phys. Rev. Lett. 68, 94 (1992).

[22]J. N. Andersen, E. Lundgren, R. Nyholm, and M. Qvarford, Surf. Sci. 289, 307 (1993).

[23]J. O. Porteus, Surf. Sci. 41, 515 (1974).

[24]A. Hohlfeld and K. Horn, Surf. Sci. 211/212, 844 (1989).

[25]J. Burchhardt, M. M. Nielsen, D. L. Adams, E. Lundgren, J. N. Andersen, C. Stampfl, M. Scheffler, A. Schmalz, S. Aminpirooz, and J. Haase, Phys. Rev. Lett. 74, 1617 (1995).

[26]C. Stampfl and M. Scheffler, Surf. Sci. Lett. 319, L23 (1994).

[27]H. Brune, J. Wintterlin, J. Trost, G. Ertl, J. Wiechers, and R. J. Behm, J. Chem. Phys. 99, 2128 (1993).

[28]J. Wintterlin, J. Wiechers, H. Brune, T. Gritsch, H. Höfer, and R. J. Behm, Phys. Rev. Lett. 62, 59 (1989).

[29]J. M. Mundelar, R. Murphy, K. D. Tsuei, and E. W. Plummer, Chem. Phys. Lett. 143, 593 (1988).

[30]J. V. Barth, R. J. Behm, and G. Ertl, Surf. Sci. 302, L319 (1994).

[31]R. Schuster, J. V. Barth, G. Ertl, and R. J. Behm, Surf. Sci. Lett. 247, L229 (1991).

[32]J. V. Barth, Ph.D. thesis, Freie Universität Berlin, 1992.

[33]G. Doyen, D. Drakova, J. V. Barth, R. Schuster, T. Gritsch, R. J. Behm, and G. Ertl, Phys. Rev. B 48, 1738 (1993).

[34]H. Brune, J. Wintterlin, G. Ertl, and R. J. Behm, Europhys. Lett. 13, 123 (1990).

[35]R. Stumpf, Ph.D. thesis, Freie Universität Berlin, 1993.

[36]C. Stampfl, M. Scheffler, H. Over, J. Burchhardt, M. M. Nielsen, D. L. Adams, and W. Moritz, Phys. Rev. Lett. **69**, 1532 (1992).

[37]T. Aruga and Y. Murata, Prog. Surf. Sci. **31**, 61 (1989).

[38]K. Müller, G. Besold, and K. Heinz, in *Physics and Chemistry of Alkali Metal Adsorption* (Ref. 4), p. 65.

[39]J. Neugebauer and M. Scheffler, Phys. Rev. Lett. **71**, 577 (1993).

[40]R. Stumpf and M. Scheffler (unpublished).

[41]M. M. Nielsen, J. Burchhard, D. L. Adams, E. Lundgren, and J. N. Andersen, Phys. Rev. Lett. **72**, 3370 (1994).

[42]G. Scragg, B. C. C. Cowie, M. Kerkar, D. P. Woodruff, A. Daimellah, S. Turton, and R. G. Jones (unpublished).

[43]N. D. Lang, Phys. Rev. B **37**, 10 395 (1988).

[44]N. D. Lang, Comm. Condens. Matter Phys. **14**, 253 (1989).

[45]D. Heskett, K.-H. Frank, E. E. Koch, and H.-J. Freund, Phys. Rev. B **36**, 1276 (1987).

[46]N. D. Lang, Phys. Rev. Lett. **56**, 1164 (1986).

[47]H. Ishida, Phys. Rev. B **40**, 1341 (1989).

[48]P. Häberle and T. Gustafsson, Phys. Rev. B **40**, 8218 (1989).

[49]R. M. Eastment and C. H. B. Mee, J. Phys. F **3**, 1738 (1973).

[50]E. D. Westre, D. E. Brown, J. Kutzner, and S. M. George, Surf. Sci. **294**, 185 (1993).

[51]G. L. Kellogg, Phys. Rev. Lett. **67**, 216 (1991).

[52]J. D. Wrigley and G. Ehrlich, Phys. Rev. Lett. **44**, 661 (1980).

[53]L. Hansen, P. Stoltze, K. W. Jacobsen, and J. K. Nørskov, Phys. Rev. B **44**, 6523 (1991).

[54]E. Ganz, S. K. Theiss, I. Hwang, and J. Golovchenko, Phys. Rev. Lett. **68**, 1567 (1992).

[55]S. C. Wang and G. Ehrlich, Phys. Rev. Lett. **67**, 2509 (1991).

[56]J. A. Gaspar, A. G. Eguiluz, K. D. Tsuei, and E. W. Plummer, Phys. Rev. Lett. **67**, 2854 (1991).

[57]K. D. Tsuei, D. Heskett, A. P. Baddorf, and E. W. Plummer, J. Vac. Sci. Technol. A **9**, 1761 (1991).

[58]J. Haase (private communication)

[59]R. Fasel, P. Aebi, J. Osterwalder, and L. Schlappbach (unpublished).